Progress in Lipid Research 101 (2026) 101361

Contents lists available at ScienceDirect

Progress in Lipid Research

journal homepage: www.elsevier.com/locate/plipres

Review Article

Properties and biochemistry of phosphatidylcholine: diacylglycerol cholinephosphotransferase

Brandon A. Ulch [a], Alyssa C. Clews [a], Caroline A. Reisiger [b], Li-Hua Zhu [c], Robert T. Mullen [a], Matthew S. Kimber [a], Yang Xu [a,*]

[a] Department of Molecular and Cellular Biology, University of Guelph, Guelph, Ontario N1G 2W1, Canada
[b] Department of Plant Agriculture, University of Guelph, Guelph, Ontario N1G 2W1, Canada
[c] Department of Plant Breeding, Swedish University of Agricultural Sciences, P.O. Box 190, SE-234 22 Lomma, Sweden

ARTICLE INFO

Keywords:
PDCT
Triacylglycerol biosynthesis
Phosphatidylcholine
Diacylglycerol
ROD1
Plant oils
Monounsaturated fatty acid
Fatty acid modification

ABSTRACT

Plant oils, primarily composed of triacylglycerols (TAGs), are essential for both food and industrial applications. TAGs consist of three fatty acids esterified to a glycerol backbone, and their value and functionality are largely determined by their fatty acid composition. Hence, enhancing the fatty acid profile of plant oils is a primary focus for improving their economic and practical potential. Phosphatidylcholine: Diacylglycerol Cholinephosphotransferase (PDCT), encoded by the *REDUCED OLEATE DESATURATION1* (*ROD1*) gene in *Arabidopsis thaliana*, catalyzes the interconversion between phosphatidylcholine, the site of fatty acid modification, and diacylglycerol, the precursor of TAG assembly. PDCT plays a key role in determining the fatty acid composition and quality of oils, making it an attractive target for engineering crops with tailored oil profiles. This review systematically examines the biochemical, genetic, and molecular biology research on PDCT over the past decades, focusing on its phylogeny, physiological roles, regulation, biochemical characterization, structural features, and biotechnological applications. We also analyze the predicted structure of PDCT, which suggests a domain-swapped homodimer configuration based on AlphaFold3 modeling, and we discuss potential catalytic mechanisms. Finally, we highlight key open questions in the field and propose future research directions.

1. Introduction

Plant oils are highly versatile lipids, mainly composed of triacylglycerols (TAGs), which consist of three fatty acids esterified to a glycerol backbone. They are used for food, feed and in the manufacturing of various commercial and consumer goods, including biodiesel, soaps, paints and plastics [1,2]. The fatty acid composition of plant oils varies significantly across different plant species, affecting their commercial value and potential applications [3]. For instance, polyunsaturated fatty acids (PUFAs), such as linoleic (C18:2,

Abbreviations: 14:0/14:0-PC, *sn*-1,2-dimyristoyl-glycero-3-phosphatidylcholine; 16:0/16:0-DAG, *sn*-1,2-dipalmitoyl-glycerol; 16:0/16:0-PC, *sn*-1,2-dipalmitoyl-glycero-3-phosphatidylcholine; 18:1/18:1-DAG, *sn*-1,2-dioleoyl-glycerol; 18:1/18:1-PC, *sn*-1,2-dioleoyl-glycero-3-phosphatidylcholine; 18:1OH, ricinoleic acid (12-hydroxy-18:1Δ^{9cis}); 18:2/18:2-DAG, *sn*-1,2-dilinoleoyl-glycerol; 18:2/18:2-PC, *sn*-1,2-dilinoleoyl-glycero-3-phosphatidylcholine; 18:3/18:3-DAG, *sn*-1,2-dilinolenoyl-glycerol; 18:3/18:3-PC, *sn*-1,2-dilinolenoyl-glycero-3-phosphatidylcholine; ARF12, AUXIN RESPONSE FACTOR12; C16:0, palmitic acid (16:0); C18:1, oleic acid (18:1Δ^{9cis}); C18:2, linoleic acid (18:2$\Delta^{9cis,12cis}$); C18:3, linolenic acid (18:3$\Delta^{9cis,12cis,15cis}$); CPS, Cyclopropane Fatty Acid Synthase; CPT, Cholinephosphotransferase; CRISPR-Cas9, clustered regularly interspaced short palindromic repeats-CRISPR associated protein 9; CTP, chloroplast transit peptide; DAG, diacylglycerol; DGAT, Diacylglycerol Acyltransferase; DPBF2, DC3 Promoter-Binding Factor2; EMS, ethyl methanesulfonate; ER, endoplasmic reticulum; FAD, Fatty Acid Desaturase; FADX, Fatty Acid Desaturase X; FAE, Fatty Acid Elongase; G3P, glycerol-3-phosphate; GC, gas chromatography; IPCS, Inositol Phosphorylceramide Synthase; L1L, LEAFY COTYLEDON1-Like; LEC1, LEAFY COTYLEDON1; LPCAT, Lysophosphatidylcholine Acyltransferase; LPAT, Lysophosphatidic Acid Acyltransferase; LPT, Lipid Phosphatase/Phosphotransferase; MBD, methyl-CpG-binding domain; MYB, myeloblastosis; MYC, myelocytomatosis; MUFA, monounsaturated fatty acid; PC, phosphatidylcholine; PDAT, Phosphatidylcholine:Diacylglycerol Acyltransferase; PDCT, Phosphatidylcholine:Diacylglycerol Cholinephosphotransferase; PLD, Phospholipase D; PUFA, polyunsaturated fatty acid; FAH, Fatty Acid Hydroxylase; RNAi, RNA interference; ROD1, Reduced Oleate Desaturation1; SFA, saturated fatty acid; SMS, Sphingomyelin Synthase; TAG, triacylglycerol; T-DNA, transfer DNA; TGD, trigalactosyldiacylglycerol; TLC, thin layer chromatography; WRI1, WRINKLED1.

* Corresponding author.
E-mail address: yangxu@uoguelph.ca (Y. Xu).

https://doi.org/10.1016/j.plipres.2025.101361
Received 30 September 2025; Received in revised form 19 November 2025; Accepted 20 November 2025
Available online 21 November 2025

18:2$^{\Delta 9cis,12cis}$) and linolenic (C18:3, 18:3$^{\Delta 9cis,12cis,15cis}$) acids, are abundant in crops, such as soybean (*Glycine* max) and flax (*Linum usitatissimum*), respectively, and play important roles in nutrition and health [4,5]. Additionally, some plant oils are rich in unusual fatty acids with industrial significance, such as ricinoleic acid (12-hydroxy-18:1$^{\Delta 9cis}$), which constitues a high proportion of castor (*Ricinus communis*) oil and is highly valued in manufacturing due to the hydroxyl groups on its acyl chains [6,7]. With a growing global population and an increasing demand on plant oils for food and industrial materials, there is a growing interest in enhancing oil production and bioengineering oil crops to produce tailored fatty acids.

In plants, oil biosynthesis starts with the *de novo* fatty acid biosynthesis in the plastids, followed by assembly into TAG in the endoplasmic reticulum (ER). Fatty acids can be modified (e.g., desaturation, hydroxylation, etc.) in the form of phosphatidylcholine (PC) via the catalysis of Fatty Acid Desaturase (FAD) family enzymes. The modified fatty acids are futher channeled to diacylglycerol (DAG) or acyl-CoA for TAG biosynthesis [3]. Phosphatidylcholine: Diacylglycerol Cholinephosphotransferase (PDCT) catalyzes the interconversion between PC and DAG, where the phosphocholine head group from PC is transferred to DAG, yielding new DAG and PC [PC1 + DAG2 ↔ PC2 + DAG1] [8]. This enables newly-synthesized fatty acids attached to DAG to enter the PC pool and be subjected to modification. Simultaneously, modified fatty acids attached to PC can be returned to the DAG pool for oil biosynthesis [8,9]. Therefore, PDCT plays an important role in affecting the fatty acid composition of TAG by interconverting modified and unmodified PC and DAG. PDCT belongs to the Lipid Phosphatase/Phosphotransferase (LPT) family, a group of integral membrane proteins that play central roles in lipid metabolism and signaling across organisms from yeasts and plants to humans [10,11]. LPT family proteins transfer phosphate-containing headgroups either between lipids or in exchange for water and are characterized by a core domain with six transmembrane-spanning α-helices [12]. While the structures and catalytic mechanisms of several LPT proteins have been elucidated [13], those of PDCT remain unknown.

Here, we provide a systematic review of PDCT with a focus on its phylogeny, physiological roles, regulation, biochemical characterization, structural features, and biotechnological applications. We also predict the structure of PDCT using AlphaFold3, which suggests a domain-swapped homodimer configuration, and based on analysis, we propose putative catalytic mechanisms for the enzyme. Finally, we highlight some key open questions in the field and propose future research directions.

2. Identification and phylogeny

An early genetic screen by the Somerville and Browse Labs for *Arabidopsis thaliana* (Arabidopsis) mutants with alterations in seed lipid fatty acid composition has identified mutations in various *FAD* and *Fatty Acid Elongase* (FAE) genes as well as a novel gene called *ROD1* (*Reduced Oleate Desaturation1*) [14]. Specifically, the *rod1* mutant (disruption in *ROD1* gene) showed a 20 % increase in C18:1 (oleic acid, 18:1$^{\Delta 9cis}$) content, with corresponding decreases in C18:2 and C18:3 [14]. In 2009, *ROD1* was discovered by Lu et al. (2009) to encode a novel enzyme in lipid biosynthesis, namely PDCT (hereafter *ROD1* and *PDCT* are referred to interchangeably), which catalyzes the transfer of C18:1-DAG into PC for desaturation and the reverse transfer of C18:2- and C18:3-PC into DAG for TAG synthesis [8]. Since its initial identification, PDCT homologs have been identified through the sequence homology to AtROD1 (Arabidopsis PDCT) and/or functionally characterized in the numerous other plant species: *R. communis* (castor) [15], *L. usitatissimum* (flax) [16], *Crambe abyssinica* (crambe) [17], *Litchi chinensis* (lychee) [18], *Brassica napus* (canola) [19], *Camelina sativa* (camelina) [9,20,21], *Helianthus annuus* (sunflower) [22], *Thlaspi arvense L.* (pennycress) [23,24], *Oryza sativa* (rice) [25,26], *Lepidium campestre* (field cress) [27], *G.* max (soybean) [28,29], and *Gossypium hirsutum* (cotton) [30,31].

To date, *PDCT* has been exclusively identified in land plant species, where at least one copy of the gene is present (Fig. 1) [10,11,16,32]. Various reports suggest that *PDCT* may be absent in some species from earlier-diverging lineages, such as the protist *Thraustochytrium* [33], the marine fungus *Schizochytrium* [34], other fungal species including *Saccharomyces cerevisiae*, *Apiospora montagnei*, *Cryphonectria parasitica*, *Didymella exigua*, *Amanita muscaria*, and *Spizellomyces pubctatus* [10], as well as both unicellular and multicellular green algae such as *Chlamydomonas reinhardtii* and *Volvox carteri* [10] and spikemoss (*Selaginella moellendorffii*) [10]. *PDCT* has also been reported to be absent in a few land plant species, including bitter melon (*Momordica charantia*) and tung tree (*Vernicia fordii*) [35]. The apparent lack of *PDCT* in these species may reflect low transcript abundance rather than true absence, as a recent study identified a PDCT ortholog in tung [36], and a putative PDCT homolog is also detectable in the NCBI non-redundant protein database for bitter melon using BLAST. Given that both bitter melon and tung accumulate high levels of α-eleostearic acid (18:3$^{\Delta 9cis,\ 11trans,\ 13trans}$), it is possible that PDCT does not play a major role in conjugated fatty acid accumulation in these plant species [35,36].

The apparent absence of *PDCT* genes in earlier-diverging lineages and their restriction to land plants indicate that *PDCT* may have emerged relatively late in plant evolution, possibly in association with the increasing importance of lipid accumulation [10]. It is not surprising that *PDCT* is absent in unicellular bacteria and in photosynthetic organisms that lack PC, as only about 15 % of bacteria are capable of synthesizing PC [37], whereas cyanobacteria appear to lack PC altogether and instead utilize phosphatidylglycerol as the predominant membrane phospholipid [38]. However, among early-diverging photosynthetic eukaryotes that contain PC as a major phospholipid and accumulate unusual or PC-modified fatty acids [39,40], evidence for the presence of *PDCT* remains inconclusive. Therefore, to gain more insights into PDCT evolution, we conducted a DELTA-BLAST search [41] against the NCBI non-redundant protein databases using the AtROD1 deduced amino acid sequence as the query. The search was limited to taxonomic groups with relatively little information on PDCT, including non-angiosperm plants, Chlorophyta (excluding plants), animals, fungi, archaea, and Gram-positive bacteria. This analysis identified various putative homologs containing the conserved SGH (C2) and HXXXD (C3) motifs, which are characteristics of PDCT and other members of the LPT protein family (Fig. 1). The phylogenetic analysis revealed none of the homologs from diatoms or green algae clustered with PDCTs; instead, they grouped with Inositol Phosphorylceramide Synthases (IPCSs) and Sphingomyelin Synthases (SMSs) (Fig. 1). Interestingly, several putative PDCT homologs from non-flowering plants clustered with previously characterized plant PDCTs, and some share all conserved motifs, including an EYT motif, which appears to be unique to PDCTs among the LPT family (Fig. 1) and may be important for its catalysis (see Section 7). However, whether these proteins exhibit PDCT activity remains unknown. A similar case was reported in the oomycete *Phytophthora infestans*, where two putative PDCTs were identified, but these proteins failed to demonstrate PDCT function, raising questions about whether they are true PDCTs or simply members of the broader LPT family [42].

3. Expression, subcellular localization and physiological functions

PDCT typically consists of three exons in dicotyledonous plants, or two in monocotyledonous plants [32], and tends to be expressed highest in developing seed and floral tissues, while also being relatively weakly expressed throughout most other plant tissues [16,22,43–50]. In the developing seeds of most plant species, the transcript level of *PDCT* increases along with oil accumulation during seed maturation and decreases back to basal levels as seed oil accumulation begins to plateau, suggesting a coordinated role with TAG accumulation [44,45,51,52]. In some species such as pennycress, *Lindera glauca*, and Siberian apricot,

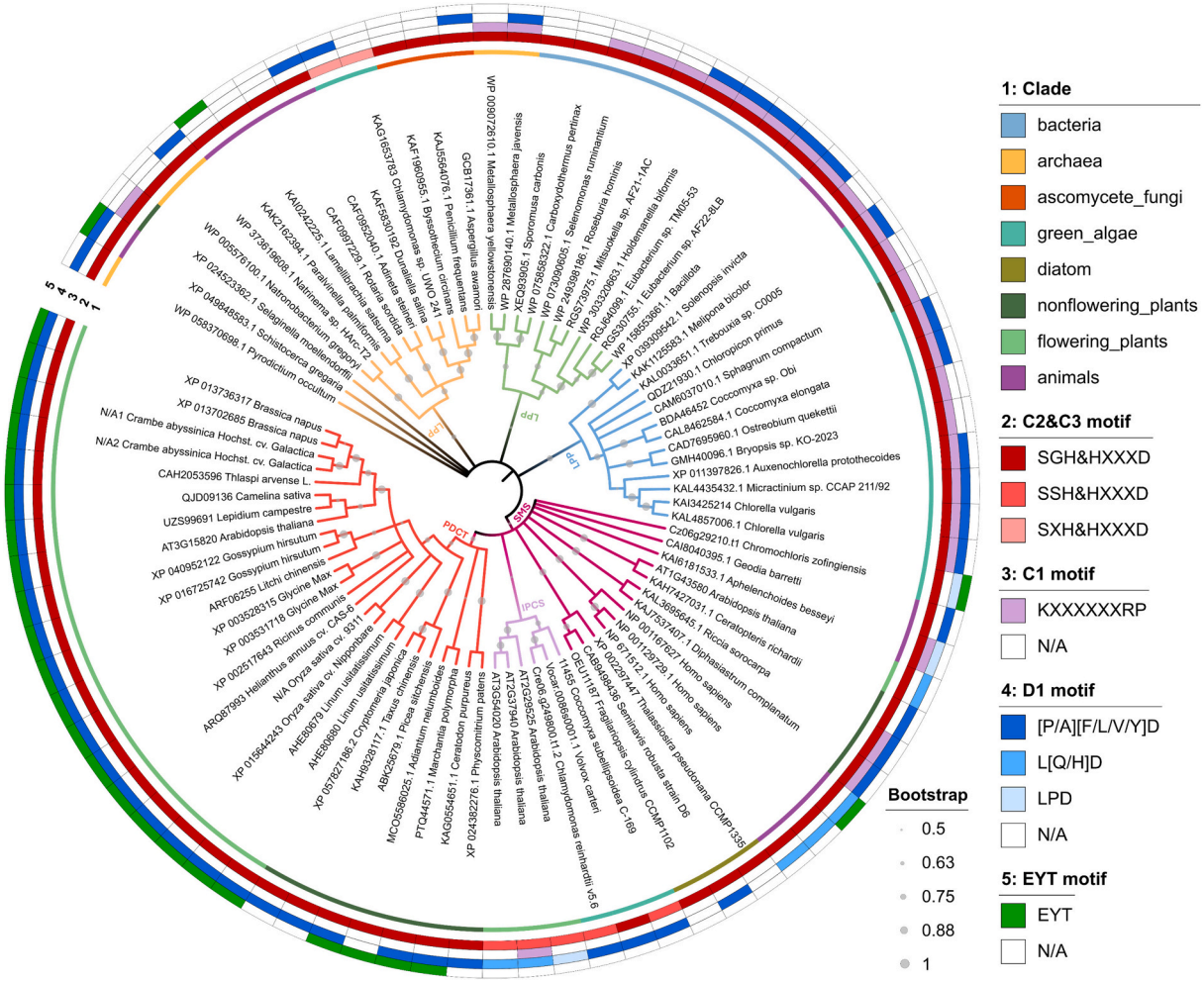

Fig. 1. Phylogenetic relationship of PDCT and other related enzymes from plants and early divergent species. The maximum likelihood phylogenetic tree with 100 bootstrap replications was constructed with MEGA11 and visualized using iTOL. The bootstrap values were represented by the size of the grey circles at the tree nodes. Clades of PDCT homologs, Inositol Phosphorylceramide Synthase (IPCS) homologs, and Sphingomyelin Synthase (SMS) homologs are shown in red, light purple, and purple, respectively. Clades of other Lipid Phosphate Phosphatase (LPP) homologs are shown in blue, green, and orange. Species/clade are shown in circle layer 1. Results of C2 and C3 motif, C1 motif, D1 motif and EYT motif analyses are shown in circle layers 2, 3, 4 and 5, respectively. A DELTA-BLAST search was performed against the NCBI non-redundant protein database using the AtROD1 sequence as the query, with the taxonomy restricted to Plants (excluding angiosperms), Chlorophyta (excluding plants), Animals, Fungi, Archaea, and Gram-positive Bacteria. Putative homologs containing the conserved SGH (C2) and HXXXD (C3) motifs, along with selected PDCT, IPCS, and SMS homologs, were included in the analysis. The accession numbers of proteins used for the construction of the phylogenetic tree are listed in Supplemental Table S1. (For interpretation of the references to colour in this figure legend, the reader is referred to the web version of this article.)

the timing and magnitude of *PDCT* expression has been reported to differ from oil accumulation and other major oil biosynthetic genes during seed or kernel development, but it typically coincides with the accumulation of PC-modified fatty acids [50,53,54]. Additionally, evidence suggests that *PDCT* isoforms are expressed in a tissue-specific manner, such as in maize, where the expression of one *PDCT* isoform is upregulated in anthers while the other is upregulated in embryonic tissues [10].

PDCT encodes a membrane-bound protein, likely associated with ER membranes, where it participates in DAG and PC interconversion and TAG biosynthesis. This is supported by the ER localization of fluorescent protein-tagged PDCTs from soybean and cotton observed via transient expression in *Nicotiana benthamiana* (tobacco) leaves [29,30]. Interestingly, PDCTs from rice and soybean have also been reported to reside at both the ER and plasma membrane when transiently expressed in *N. benthamiana* leaves [25], and to the plasma membrane when expressed in Arabidopsis leaf mesophyll protoplasts [28], respectively. It is still unknown whether the plasma membrane localization reflects an artifact of the transient expression system employed or points to a specific functional role for PDCT at the plasma membrane.

As a mediator of acyl flux through the bidirectional channeling of fatty acids between PC and DAG, PDCT plays a key role in determining the ratio of PUFAs relative to monounsaturated (MUFAs) and saturated fatty acids (SFAs) in lipids of tissues where it is predominantly expressed. This is exemplified by a wide range of plant species where altered *PDCT* expression leads to shifts in the relative composition of C18 fatty acids (Table 1). More specifically, *rod1* mutants demonstrate an increase of C18:1 with a relative decrease of C18:2 and C18:3 in seed total lipids (primarily TAG), whereas an inverse trend was generally reported following *PDCT* overexpression (Table 1). For example, in Arabidopsis *rod1* seeds C18:1 increases from 15.1 % to 32.8 % while C18:2 and C18:3 decrease from 29.2 % to 13.8 % and from 19.9 % to 15.6 %, respectively, compared with wild-type plants [8]. In contrast, overexpression of flax *PDCT* in Arabidopsis reduces C18:1 from ~18 % to 12 % and increases C18-PUFA (C18:2 and C18:3) content from ~43 % to 50–52 % [16]. As for seed PC, an increase in C18:1 content from 17 % to 22 % and a slight reduction in C18:2 content from 47 % to 45 %, but no apparent change in C18:3 (~15 %), were observed in Arabidopsis *rod1* [55]. Despite changes in seed lipid composition, PDCT appears to

Table 1
Overview of bioengineering strategies using PDCT to produce oils with tailored fatty acid profile.

Organism	Target(s)	Method	Significant fatty acids (Mol% or notes)	Seed oil content and other agronomic impact(s)	Ref
Knocking out *PDCT* to improve monounsaturated fatty acid content in seeds (or in other tissues for other purposes when noted; compared to wild type)					
Arabidopsis thaliana	*rod1*	EMS	Total seed lipids ↑↑ C18:1: 15.1 % to 32.8 % ↓↓ C18:2: 29.2 % to 13.8 % ↓ C18:3: 19.9 % to 15.6 % ↑ C20:1: 18.6 % to 20.6 % Seed TAG ↑↑ C18:1: 17.9 % to 39.1 % ↓↓ C18:2: 30.5 % to 14.2 % ↓ C18:3: 16.2 % to 12.3 % ↓ C20:1: 18.6 % to 17.9 %	N/A	[8]
Crambe abyssinica	*pdct1* + *pdct2*	RNAi gene silencing	Total seed lipids ↑ C18:1: ~ 14 % to 18 % ↓ C18:2: ~ 7 % to 5 %	N/A	[17]
Brassica napus	*rod1.a3 or rod1.c3*	EMS	Total seed lipids (unit not specified, mol or mass%) ↑ C18:1: ~ 60 % to 62 % ↓ C18:2: ~ 20 % to 19 %	N/S	[19]
	rod1.a3 + *rod1.c3*	EMS mutant crossing	Total seed lipids (unit not specified, mol or mass%) ↑ C18:1: ~ 60 % to 67 % ↓ C18:2: ~ 20 % to 14 %		
	rod1.a3 + *rod1.c3*	RNAi gene silencing	Total seed lipids (unit not specified, mol or mass%) ↑ C18:1: ~ 61 % to 68 % ↓ C18:2: ~ 19 % to 12 %		
Thlaspi arvense L.	*rod1*	EMS	Total seed lipids ↑↑ C18:1: ~ 10 % to 22 % ↓↓ C18:2: ~ 18 % to 10 %	N/A	[23]
Thlaspi arvense L.	*rod1*	CRISPR-Cas9	Seed TAG ↑↑ C18:1: ~ 12 % to 23 % ↓↓ C18:2: ~ 19 % to 9 %	N/S	[24]
Lepidium campestre	*rod1*	CRISPR-Cas9	Seed TAG ↑↑ C18:1: ~ 13 % to 22 % ↓ C18:2: ~ 9 % to 8 % ↓ C18:3: ~ 38 % to 30 %	N/A	[27]
Glycine max (L.) Merr.	*pdct1* + *pdct2*	CRISPR-Cas9	Total seed lipids (mass%) ↓ C18:0: ~ 5 % to 4 % ↑↑ C18:1: ~ 16 % to 45 % ↓↓ C18:2: ~ 56 % to 38 % ↓↓ C18:3: ~ 10 % to 0.3 %	N/S	[28]
Gossypium hirsutum	*pdct1* + *pdct2*	CRISPR-Cas9	Total seed lipids (unit not specified, mol or mass%) ↑ C16:0: ~ 21 % to 26 % ↑ C18:0: ~ 1.7 % to 2.4 % ↑ C18:1: ~ 14.5 % to 16.5 % ↓ C18:2: ~ 60 % to 53 %	N/S	[31]
Gossypium hirsutum (cv. Jimian14)	*pdct1*	RNAi gene silencing	Total fiber lipids ↓ C16:0: ~ 40 % to 39 % ↑ C18:2: 12.91 % to 15.25–17.21 % ↓ C18:3: ~ 40 % to 38 %	Increased fiber fineness, length and strength	[30]
Oryza sativa L.	*lin6 (pdct)*	CRISPR-Cas9	Whole grain lipids (mg/g dry weight) ↑ C18:1: ~ 9 to 11 mg/g ↓ C18:2: ~ 12 to 10 mg/g	N/A	[26]
Oryza sativa L.	*lin6 (pdct)*	CRISPR-Cas9	Whole grain lipids ↑ C18:1: ~ 32 % to 36 % ↓ C18:2: ~ 30 % to 25 %	Increased total fatty acid content (~ 27 to 35–42 mg/100 g seed), increased grain length and longitudinal epidermal cell number and length, decreased grain weight and thickness	[56]

(*continued on next page*)

Table 1 (*continued*)

Organism	Target(s)	Method	Significant fatty acids (Mol% or notes)	Seed oil content and other agronomic impact(s)	Ref
Knocking out *PDCT* in combination with knocking out other genes to improve monounsaturated fatty acid content in seeds (compared to wild type)					
A. thaliana	*lpcat1* + *lpcat2*	T-DNA insertion mutant	Total seed lipids (mass%) ↓ C18:1: 14.7 % to 13.0 % ↓ C18:2: 27.8 % to 25.3 % ↓ C18:3: 20.0 % to 18.0 % ↑ C20:1: 19.9 % to 25.3 % ↑↑ C22:2: 1.8 % to 3.3 %	N/A	[55]
	rod1 + *lpcat1* + *lpcat2*	mutant crossing	Total seed lipids (mass%) ↑↑ C18:1: 14.7 % to 42.4 % ↓↓ C18:2: 27.8 % to 7.4 % ↓↓ C18:3: 20.0 % to 9.0 % ↑ C20:1: 19.9 % to 26.1 % ↓↓ C22:2: 1.8 % to 0.6 %		
C. abyssinica	*lpcat1–1* + *lpcat1–2*	RNAi gene silencing	Total seed lipids ↑ C18:1: ~ 14 % to 19 % ↑↑ C20:1: ~ 1 % to 6 % ↓↓ C22:1: ~ 60 % to 48 %	N/A	[17]
	pdct1 + *pdct2* + *lpcat1–1* + *lpcat1–2*		Total seed lipids ↑ C18:1: ~ 14 % to 22 % ↓ C18:2: ~ 7 % to 5 % ↑↑ C20:1: ~ 1 % to 8 % ↓↓ C22:1: ~ 60 % to 48 %		
Thlaspi arvense L.	*fae1*	EMS	Total seed lipids ↑↑ C18:1: ~ 10 % to 40 % ↑↑ C18:2: ~ 18 % to 32 % ↑ C18:3: ~ 13 % to 18 % ↓↓ C20:1: ~ 10 % to 1 % ↓↓ C22:1: ~ 39 % to 0 % ↓↓ C24:1: ~ 3 % to 0 %	N/A	[23]
	rod1 + *fae1*		Total seed lipids ↑↑ C18:1: ~ 10 % to 61 % ↓↓ C18:2: ~ 18 % to 12 % ↑↑ C18:3: ~ 13 % to 18 % ↓↓ C20:1: ~ 10 % to 1 % ↓↓ C22:1: ~ 39 % to 0 % ↓↓ C24:1: ~ 3 % to 0 %		
Thlaspi arvense L.	*fae1*	CRISPR-Cas9	Seed TAG ↑↑ C18:1: ~ 12 % to 48 % ↑↑ C18:2: ~ 19 % to 28 % ↑↑ C18:3: ~ 12 % to 18 % ↓↓ C20:1: ~ 12 % to 1 % ↓↓ C22:1: ~ 35 % to 0 % ↓↓ C24:1: ~ 3 % to 0 %	Decreased seed TAG content	[24]
	rod1 + *fae1*		Seed TAG ↑↑ C18:1: ~ 12 % to 60 % ↓ C18:2: ~ 19 % to 17 % ↑↑ C18:3: ~ 12 % to 19 % ↓↓ C20:1: ~ 12 % to 0 % ↓↓ C22:1: ~ 35 % to 0 % ↓↓ C24:1: ~ 3 % to 0 %	Decreased seed TAG content	
Knocking out *PDCT* in combination with OE other genes to prepare structured lipids in seeds					
A. thaliana	*AtLPAT1ΔCTP in rod1*	seed-specific *glycinin* promoter	Seed TAG – compared to *AtLPAT1ΔCTP* expressed in wild type ↑↑ Ratio of C16:0 at *sn*-2 vs *sn*-1 + 3: ~30 % to 56 %	N/S	[83]
	AtLPAT1ΔCTP in rod1/lpcat2–3		Seed TAG – compared to *AtLPAT1ΔCTP* expressed in wild type ↑↑ Ratio of C16:0 at *sn*-2 vs *sn*-1 + 3: ~30 % to 71 %	Decreased seed TAG content than wild type	
Overexpression (OE) of *PDCT* (and other genes) to improve polyunsaturated fatty acid content in seeds (or in other tissues/organisms when noted; compared to wild type)					
A. thaliana	*LuPDCT1 or LuPDCT2*	seed-specific *napin* promoter	Total seed lipids ↓↓ C18:1: 18.77 % to 12.08 or 12.04 % ↑ C18:2: 26.90 % to 29.28 or 29.11 % ↑ C18:3: 16.31 % to 20.87 or 22.47 %	N/A	[16]

(*continued on next page*)

Table 1 (*continued*)

Organism	Target(s)	Method	Significant fatty acids (Mol% or notes)	Seed oil content and other agronomic impact(s)	Ref
Saccharomyces cerevisiae YNL130C	*LuFAD2* + *LuFAD3*	*Gal1* promoter	Yeast TAG – compared to yeast expressing the empty vector ↑ C16:0: 10.17 % to 11.99 % ↑ C16:1: 49.17 % to 51.58 % ↓ C18:1: 36.63 % to 32.38 %	N/A	[16]
	LuFAD2 + *LuFAD3* + *LuPDCT1 or LuPDCT2*		Yeast TAG – compared to yeast expressing the empty vector ↑ C16:0: 10.17 % to 13.0 or 12.56 % ↓ C16:1: 49.17 % to 42.29 or 45.58 % ↑↑ C16:2: 0 % to 2.56 or 1.66 % ↑ C18:0: 4.03 % to 6.56 or 5.66 % ↓↓ C18:1: 36.63 % to 24.09 or 26.93 % ↑↑ C18:2: 0 % to 4.57 or 2.75 % ↑↑ C18:3: 0 % to 6.64 or 4.85 %		
Oryza sativa L.	*OsLIN6*	Native promoter	Total grain lipids [mg/g DW] ↓ C18:1: ~ 11 to 9 mg/g ↑ C18:2: ~ 11 to 13 mg/g	N/A	[26]
Camelina sativa	*CsPDCT*	seed-specific *phaseolin* promoter	Total seed lipids ↑ C18:1: ~ 13 % to 16 % ↓ C18:2: ~ 20 % to 17 % ↑ C18:3: ~ 36 % to 37 %	Increased seed oil content (34 % to 37.5 %), and seed yield	[21]
Gossypium hirsutum (cv. Jimian14)	*GhROD1*	35S promoter	Total fiber lipids ↑ C16:0: ~40 % to 42 % ↑↑ C18:0: 1.33 % to 2.37–2.67 % ↓↓ C18:1: 4.26 % to 2.71–2.9 % ↓ C18:2: ~13 % to 10 %	N/S	[30]
Overexpression (OE) of *PDCT* (and other genes) to improve unusual fatty acid content in seeds (or in other tissues/organisms when noted)					
A. thaliana	*OE RcFAH12* in *rod1*	seed-specific *glycinin, napin* and *phaseolin* promoters	Total seed lipids (mass%) HFA: 5.5 %	~38 % reduction in seed oil content compared to wild type	[15]
	OE RcFAH12 + *RcROD1* in *rod1*		Total seed lipids (mass%) HFAs: 9.7 %	~12 % reduction in seed oil content compared to wild type	
	OE RcFAH12 in wild type		Total seed lipids (mass%) HFAs: 9.9 %	N/S	
	OE RcFAH12 + *RcROD1* in wild type		Total seed lipids (mass%) HFAs: 19.9 %	N/S	
	OE RcFAH12 in *fae1*		Total seed lipids (mass%) HFAs: 17.2 %	~40 % reduction in seed oil content compared to wild type	
	OE RcFAH12 + *RcROD1* in *fae1*		Total seed lipids (mass%) HFAs: 23.3 %	~27 % reduction in seed oil content compared to wild type	
	OE RcFAH12 + *RcDGAT2* in *fae1*		Total seed lipids (mass%) HFAs: 24.7 %	N/S	
	OE RcFAH12 + *RcROD1* + *RcDGAT2* in *fae1*		Total seed lipids (mass%) HFAs: 28.5 %	N/S	
A. thaliana	*OE RcFAH12* + *RcDGAT2* + *RcPDAT1–2* + *RcPDCT*+ *RcLPCAT* in wild type	seed-specific *phaseolin*, Arabidopsis *FAE1*, and *napin* promoters	Total seed lipids HFAs: 25.3–27.2 %	Reduced seed oil content per dry weight and per seed, slightly reduced seed weight and size, delayed seed germination	[79]
	OE RcFAH12 + *RcDGAT2* + *RcPDAT1–2* + *RcPDCT*+ *RcLPCAT* in *fae1*		Total seed lipids HFAs: 27.6–28.9 %	Reduced seed oil content per dry weight but increase oil content per seed, increased seed weight and size, delayed seed germination	

(*continued on next page*)

Table 1 (*continued*)

Organism	Target(s)	Method	Significant fatty acids (Mol% or notes)	Seed oil content and other agronomic impact(s)	Ref
Camelina sativa	*OE Escherichia coli CPS* in *fad2/fae1*	seed-specific *glycin* promoter	Seed TAG (unit not specified, mol or mass%) CFAs: 4.2 %	Slightly decreased seed weight compared to *fad2/fae1*	[18]
	OE lyche LcPDCT1 + *EcCPS* in *fad2/fae1*		Seed TAG (unit not specified, mol or mass%) CFAs: 5.8 %	Slightly increased seed weight compared to *fad2/fae1*	
Nicotiana benthamiana	*OE VgFAD2-like*	*35S* promoter	Total leaf lipids (unit not specified, mol or mass%) EFAs: 8.6 %	N/A	[80]
	OE VgPDCT + *VgFAD2-like*		Total leaf lipids (unit not specified, mol or mass%) EFAs: 8.2 %		
S. cerevisiae BY4741-*snf2Δ*	*OE pomegranate PgFADX* + *PgPDAT* + *PgPDCT*	*Gal1* promoter + linoleic acid feeding	Total yeast lipids (unit not specified, mol or mass%) PuA: 3.3 %	N/A	[81]
S. cerevisiae BY4741-*snf2Δ*	*OE pomegranate PgFADX* + *PgFAD2* + *PgPDCT* + *PgLPCAT* + *PgDGAT2.c* + *Rattus norvegicus ELO2*	CRISPR-Cas9 assisted Ty retrotransposon-targeted random gene shuffling	PuA in total yeast lipids (unit not specified, mol or mass%): 26.7 % PuA in yeast TAG (unit not specified, mol or mass%): 22.4 %	N/A	[82]

↑ and ↓ indicate increases and decreases in fatty acid content, respectively; double arrows (↑↑/↓↓) denote >1.5-fold changes. N/A and N/S indicate data not available and non-significant, respectively, as reported in the references.

Abbreviations: CPS, cyclopropane fatty acid synthase; CTP, chloroplast transit peptide; CRISPR-Cas9, clustered regularly interspaced short palindromic repeats-CRISPR associated protein 9; DGAT2, diacylglycerol acyltransferase 2; EFA, epoxy fatty acid; ELO2, elongation of very-long-chain fatty acids protein 2; EMS, ethyl methanesulfonate; FAD2, fatty acid desaturase 2; FADX, fatty acid desaturase X; FAE, fatty acid elongase; FAH12, fatty acid hydroxylase 12; HFA, hydroxy fatty acid; LIN6, linoleate isomerase 6; LPAT, lysophosphatidic acid acyltransferase; LPCAT, lysophosphatidylcholine acyltransferase; PDAT, phospholipid:diacylglycerol acyltransferase; PDCT, phosphatidylcholine:diacylglycerol cholinephosphotransferase; PuA, punicic acid; ROD1, reduced oleate desaturation 1; RNAi, RNA interference; T-DNA, transfer DNA.

have no essential role in overall seed development, as seed morphology, germination rate, and total oil content of most *pdct* mutant and *PDCT* overexpression plants are indistinguishable from those of the wild type (Table 1). However, exceptions were observed in the *pdct* mutant rice and *PDCT*-overexpressing camelina. In rice, *pdct* mutant grains were reported to exhibit altered epidermal morphology, increased total fatty acid content, and reduced grain weight [56], while overexpression of *CsPDCT* in camelina seeds appears to increase seed oil content, seed yield, and both silique and seed number per plant [21].

Apart from seeds, PDCT appears to play a minimal role in other plant tissues, as only minor effects have been reported in Arabidopsis seedlings and cotton seed fibers [30,57]. In Arabidopsis *rod1* mutants, lipid profiles of leaves, roots and seedlings and physiological traits (fresh weight and rosette size) were similar to wild type [8,57]. However, when the *rod1* mutation was combined with *trigalactosyldiacylglycerol1* (*tgd1*), which exhibits increased fatty acid synthesis and flux through PC to TAG due to a block in chloroplast lipid import, the *rod1 tgd1* double mutant displayed smaller rosettes and a 30 % reduction in seedling TAG levels with increased SFA and MUFA and decreased PUFA compared to *tgd1*. These results suggest that ROD1 contributes partially to the polyunsaturated DAG pool used for TAG synthesis in *tgd1* seedlings [57]. In cotton fibers, the overexpression of *PDCT* and loss of *rod1* resulted in a slight increase in C18:0 (from 1.3 % to 2.4–2.7 %) and a decrease in C18:1 (from 4.3 % to 2.7–2.9 %), and alternatively, an increase in C18:2 (from 12.9 % to 15.2–17.2 %), respectively [30]. In the *rod1* mutant, cotton fiber thickness also decreased overall, as their length and strength modestly increased [30]. These changes to the physical properties of *rod1* cotton fibers are attributed to a cascading stress-like response, in which the relative increase of C18:2 content induces the upregulation of small-heat-shock proteins, in turn reducing hydrogen peroxide accumulation and decreasing cell wall deposition [30]. These results support a role for PDCT in modulating polar lipid composition in vegetative tissues and further hint at its involvement in stress responses, although little is known about the stress-responsive expression and transcriptional regulation of *ROD1*, as discussed below.

4. Transcriptional and post-translational regulation

The regulation of PDCT has been only minimally investigated to date and appears to occur at both transcriptional and post-translational levels (Fig. 2). At the transcriptional level, the expression of *PDCT* has been found to be affected by several transcription factors, including Wrinkled1 (WRI1), Myeloblastosis (MYB)-domain protein 89 (MYB89), Auxin Response Factor 12 (ARF12), DC3 Promoter-Binding Factor2 (DPBF2), and Leafy Cotyledon (LEC)1-Like (L1L) (Fig. 2). WRI1 is one of the key transcription factors in oil biosynthesis [58] and is an activator of *PDCT* expression. It has been shown that *PDCT* is downregulated in Arabidopsis *wri1 wri3 wri4* triple mutants [59]. Meanwhile, *PDCT* is markedly upregulated in *N. benthamiana* leaves transiently expressing different *WRI1* homologs [60] and in Arabidopsis seeds stably overexpressing *AtWRI1* [61]. This regulation is likely mediated through the direct binding of WRI1 to an AW box (CtTgGaaatctcCG) located upstream of the *PDCT* transcription start site [61]. In contrast to WRI1, MYB89 acts as a repressor of *PDCT*, whereby the expression of *PDCT* is significantly increased in Arabidopsis *myb89* mutant seeds [62]. This is likely caused indirectly by the suppression of *WRI1* via MYB89, as MYB89 binds to the promoter of *WRI1* to reduce its transcription [62]. In rice, it has been shown that *PDCT* expression is directly activated by ARF12, which binds to a transcription factor binding site (GGGACA) upstream of the promoter region of *PDCT* (*OsLIN6*) [56].

PDCT expression may also be regulated by DPBF2 and L1L, although whether this occurs through direct or indirect mechanisms is unknown. The expression of *PDCT* is slightly increased in the *dpbf2–1* mutant but highly increased in seed-specific overexpression lines of *DPBF2* in

Arabidopsis [63]. Based on a protoplast transcriptional activation assay in *N. benthamiana,* this activation was shown to occur when DPBF2 is complexed with L1L and NUCLEAR FACTOR-YC2 [63]. In soybean, a *Phospholipase Dα1* (*PLDα1*) knockdown results in an increase in *GmPDCT1* and *GmPDCT2* expression during seed development, which is likely due to changes in the phosphatidic acid pool altering the flux of available lipids and in turn activating upregulation of *PDCT* [49]. Transcriptome analyses of pepper (*Capsicum annuum*) revealed that *PDCT* exhibits differential expression during flower and fruit development possibly due to the antagonistic formation of a natural antisense transcript pair via partial overlap with *methyl-CPG-binding domain 10 (MBD10)* [64]. In silico analysis of *PDCT* across different species also identified various other stress and light-response elements in the promoter region, such as Myelocytomatosis 73 (MYC73), several G-box species, a Box 4 element, and a GT1-motif [32], but further experimental verification is required. Indeed, while there is some limited evidence that *PDCT* expression, or the expression of its transcriptional regulators, are affected by stresses, including drought, salinity, light and cold stress [32,47], in other studies there is no evidence of expressional changes, including in response to heat stress [65].

Research into the regulation of PDCT at the protein level is still in an early stage. Studies of related LPT-family proteins have hinted that its members may function as a monomer or multimer, with phosphotransferase activity occurring within the internal cavity of each protomer [11,13,66]. However, recent modeling suggests PDCT may function as a homodimer via N-terminal domain swapping (see Section 7 for additional details), or even as a heterodimer between different PDCT isoforms (PDCT1 and PDCT2) in some species [29]. PDCT may also assemble into larger oligomeric complexes through interactions with other proteins (Fig. 2). For example, PDCT has been found to interact with other lipid biosynthetic enzymes, including soybean and castor Diacylglycerol Acyltransferase 2 (DGAT2), which interact with AtROD1 in membrane yeast two hybrid (MYTH) assays [67]. Additionally, both MYTH and bimolecular fluorescence complementation (BiFC) assays examining flax PDCT have shown it may interact with itself, flax DGAT2, and Lysophosphatidylcholine Acyltransferase 2 (LPCAT2) [68]. These interactions provide preliminary evidence that PDCT could be part of larger oligomeric assemblies and/or engage in transient complexes with other proteins, facilitating the efficient transfer of fatty acids from PC or DAG to TAG. However, structural evidence to support these interactions is currently lacking.

5. *In vitro* enzyme assays and enzyme characteristics

The activity of PDCT from various plant species has been characterized *in vitro* using microsomes from *S. cerevisiae* expressing the recombinant proteins (Table 2). For these assays, *cpt1* deficient *S. cerevisiae* strains such as HJ091 (*cpt1::LEU2 ept1*) and YNL130C (*MATα cpt1:: KanMX ept1*), which lack cholinephosphotransferase (CPT) activity are commonly used. These reactions also typically use [^{14}C]-radiolabeled PC or DAG as substrates, followed by thin layer chromatography (TLC) separation and quantification of the radioactivity in the newly-formed DAG or PC [8,15,16,19,22,42]. Alternatively, assays using unlabeled PC and DAG in combination with TLC separation and gas chromatography (GC) quantification have also been reported [29]. In addition, PDCT activity has been assayed using microsomes prepared from the *S. cerevisiae* strain H1246 (*MATα are1*-Δ::*HIS3, are2*-Δ::*LEU2, dga1*-Δ::*KanMX4, lro1*-Δ::*TRP1 ADE2*) with [^{14}C]glycerol-3-phosphate (G3P) and unlabeled acyl-CoA as substrates [20,69]. This strain lacks DAG-acylating enzymes [70], resulting in DAG as the sole radioactive end product from the acylation of [^{14}C]G3P with exogenous or endogenous acyl-CoA. Therefore, radiolabeled PC is produced only when PDCT is active in the microsomal preparations [20,69]. Across these studies, PDCT activity has been assayed at pH 6.5–7.5 and 15–30 °C, using 20–250 μg of microsomal protein for 5–120 min, with measured enzyme activities ranging from ~0.001 to 5.3 nmol/mg microsomal protein/min (Table 2). The activity of plant PDCT is largely influenced by pH, with Arabidopsis PDCT (AtROD1) exhibiting optimal activity at pH 6.5–7 [8].

PDCT has not yet been well-characterized using microsomal preparations from plant tissues. In developing camelina seeds, microsomes incubated with [^{14}C]G3P and acyl-CoA exhibited a strong flux of radioactivity into PC, suggesting the presence of PDCT activity [71]. In camelina lines overexpressing *PDCT*, embryos incubated with [^{14}C]

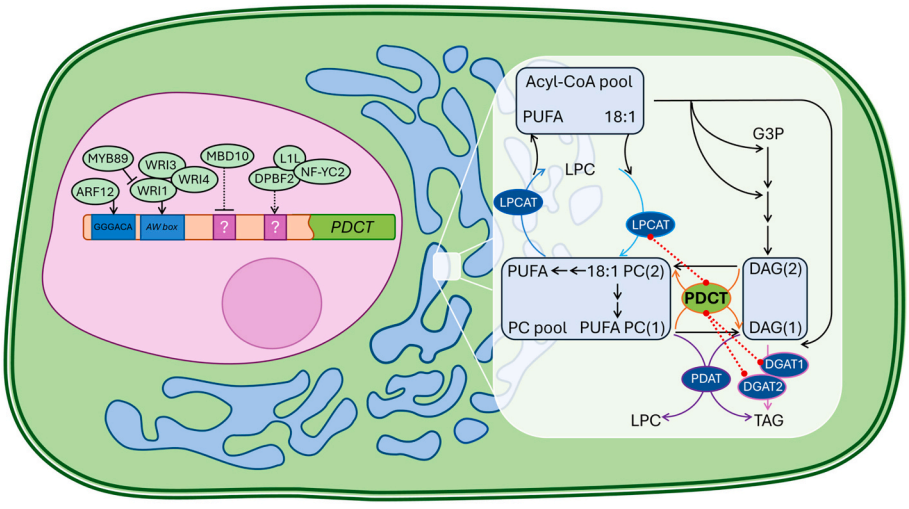

Fig. 2. Transcriptional and post-translational regulation of PDCT. Left side in nucleus (pink): Direct interactions observed for the transcriptional regulation of *PDCT*. Dotted lines indicate an observation lacking experimental confirmation or mechanism, while solid lines indicate regulators with experimental evidence. Right side in ER (blue; beige box shows a zoomed-in region): Lipid biosynthetic pathways and suggested post-translational regulation (protein-protein interactions) of PDCT. Red dotted lines indicate proteins interacted with PDCT using membrane yeast two hybrid and/or bimolecular fluorescence complementation assays. Abbreviations: ARF12, auxin response factor 12; DAG, diacylglycerol; DGAT, diacylglycerol acyltransferase; DPBF2, DC3 promoter-binding factor 2; G3P, glycerol-3-phosphate; LPC, lysophosphatidylcholine; LPCAT, lysophosphatidylcholine acyltransferase; L1L, leafy cotyledon1-like; MBD10, methyl-CpG-binding domain 10; MYB89, myeloblastosis-domain protein 89; NF-YC2, nuclear factor YC2; PC, phosphatidylcholine; PDAT, phosphatidylcholine:diacylglycerol acyltransferase; PDCT, phosphadidylcholine:diacylglycerol cholinephosphotransferase; PUFA, polyunsaturated fatty acid; TAG, triacylglycerol; WRI, wrinkled. (For interpretation of the references to colour in this figure legend, the reader is referred to the web version of this article.)

Table 2
Overview of studies examining *in vitro* PDCT activity.

Species	Enzyme	Activity (nmol/mg/min), relative activity, or notes	Reaction substrates	Detected products	Detection method	Reaction time, microsome protein amount & reaction volume	Reaction temperature & buffer	*Saccharomyces cerevisiae* strains & plasmids	Ref
A. thaliana	AtROD1	0.3	1.8 nmol [^{14}C-glycerol]18:1/18:1-DAG + 200 nmol 18:1/18:1-PC (1 mM)	PC	TLC + Radiography	15 min 20–250 μg 200 μL	15 °C MOPS (pH 6.5–7) reaction buffer	HJ091 p424 GPD	[8]
		0.04	1.8 nmol [^{14}C-glycerol]18:1/18:1-DAG	PC					
		Active	1 nmol [^{14}C-choline]14:0/14:0-PC, 100 nmol 18:1/18:1-PC +100 nmol 18:1/18:1-DAG	18:1/18:1-PC					
Phytophothora infestans	PiPDCT1	Inactive	1.8 nmol [^{14}C-glycerol]18:1/18:1-DAG + 100 nmol 18:1/18:1-PC	PC	TLC + Radiography	15 min 100 μg 200 μL	Room Temp MOPS (pH 7.5) reaction buffer	INVSc1 pYES2.0	[42]
	PiPDCT2	Inactive							
A. thaliana *Ricinus communis*	AtROD1	3.5	1.8 nmol [^{14}C-glycerol]18:1/18:1-DAG + 200 nmol soy PC (1 mM)	PC	TLC + Radiography	15 min 20–250 μg 200 μL	15 °C MOPS (pH 7.5) reaction buffer	HJ091 p424 GPD	[15]
	RcROD1	5.3							
	AtROD1	1.4	1.8 nmol [^{14}C-glycerol]18:1/18:1-DAG + 200 nmol 18:1OH-PC (1 mM)						
	RcROD1	2.0							
L. usitatissimum L.	LuPDCT1	~0.0024	0.5 nmol [^{14}C-glycerol]18:1/18:1-DAG + 2.5 nmol 18:1/18:1-DAG + 100 nmol 18:1/18:1-PC	PC	TLC + Radiography	5–15 min 100 μg 200 μL	30 °C MOPS (pH 7.5) reaction buffer	YNL130C pYES2	[16]
	LuPDCT2	~ 0.0055							
	LuPDCT1	~0.0021	2.5 nmol *sn*-1-16:0-*sn*-2-[^{14}C]18:1-PC, 10 nmol *sn*-1-16:0-*sn*-2-18:1-PC +100 nmol of 18:1/18:1-DAG	DAG					
	LuPDCT2	~0.0030							
Brassica napus	BnROD1.A3	Active (100 %)	1.8 nmol [^{14}C-glycerol]18:1/18:1-DAG + 200 nmol PC (1 mM)	PC	TLC + Radiography	15 min 20–250 μg 200 μL	15 °C MOPS (pH 7.5) reaction buffer	HJ091 p424 GPD	[19]
	BnROD1.C3	Active (100 %)							
	BnROD1.A5	Inactive							
	BnROD1.C5	Inactive							
	BnROD1.A3 R146K	Active (14 %)							
	BnROD1.A3 T150I	Inactive (3 %)							
	BnROD1.A3 G161S	Inactive (0 %)							
	BnROD1.C3 R144K	Active (100 %)							
	BnROD1.C3 G159D	Inactive (0 %)							
	BnROD1.C3 P170S	Active (15 %)							
	BnROD1.C3 E142K	Inactive (4 %)							
	BnROD1.C3 T133M	Active (100 %)							
Camelina sativa	CsPDCT1	~0.23	12.5 nmol [^{14}C]G3P + 25 nmol 18:1-CoA	PC	TLC + Radiography	60 min 100 μg 50 μL	30 °C Tris (pH 7.2) reaction buffer	H1246 pYES2-NT	[20]
		~0.10	12.5 nmol [^{14}C]G3P + 25 nmol 18:2-CoA						
		~0.29 (100 %, 1 nmol PC radioactivity)	12.5 nmol [^{14}C]G3P + 25 nmol 18:3-CoA						
		~0 % (0, nmol PC radioactivity)	12.5 nmol [^{14}C]G3P + 25 nmol 18:1OH-CoA	PC					
		~80 % (0.8 nmol PC radioactivity)	12.5 nmol [^{14}C]G3P + 20 nmol 18:3-CoA, 5 nmol 18:1OH-CoA						

(*continued on next page*)

Table 2 (*continued*)

Species	Enzyme	Activity (nmol/mg/min), relative activity, or notes	Reaction substrates	Detected products	Detection method	Reaction time, microsome protein amount & reaction volume	Reaction temperature & buffer	*Saccharomyces cerevisiae* strains & plasmids	Ref
		~15 % (0.15 nmol PC radioactivity)	12.5 nmol [^{14}C]G3P + 10 nmol 18:3-CoA, 15 nmol 18:1OH-CoA						
Helianthus annuus	HaPDCT1	0.03	12.5 nmol *sn*-1-18:1-*sn*-2-[^{14}C]-18:1-PC + 100 nmol 18:1/18:1-DAG	DAG	TLC + Radiography	30–120 min 50–200 μg 200 μL	30 °C MOPS (pH 7.5) reaction buffer	HJ091 p423 GPD	[22]
		~0.004	12.5 nmol *sn*-1-18:1-*sn*-2-[^{14}C]-18:1-PC + 100 nmol 18:1/18:1-DAG						
		~0.0025	12.5 nmol *sn*-1-18:1-*sn*-2-[^{14}C]-18:1-PC + 100 nmol 18:2/18:2-DAG						
		~0.0015	12.5 nmol *sn*-1-18:1-*sn*-2-[^{14}C]-18:2-PC + 100 nmol 18:1/18:1-DAG						
		~0.0032	12.5 nmol *sn*-1-18:1-*sn*-2-[^{14}C]-18:2-PC + 100 nmol 18:2/18:2-DAG						
C. sativa	CsPDCT1	~2.8	16 nmol *sn*-1,2-[^{14}C]18:1/18:1-DAG	PC	TLC + Radiography	5–10 min 60 μg 100 μL	30 °C phosphate buffer (pH 7.2)	H1246 pYES2-NT	[9]
		~1.5	16 nmol *sn*-1,2/2,3-rac-[^{14}C]18:1/18:1-DAG	PC					
		~1.3	6 nmol [^{14}C]18:1/18:1-PC	DAG					
	CsPDCT1	~100 % 18:1-PC ~100 % 18:2-PC ~70 % 18:3-PC	5.3 nmol [^{14}C]18:1/18:1-DAG, 5.3 nmol [^{14}C]18:2/18:2-DAG, 5.3 nmol [^{14}C]18:3/18:3-DAG	18:1/18:1-PC, 18:2/18:2-PC, 18:3/18:3-PC	Trans-methylation + Argentation TLC + Radiography				
	CsPDCT1	~100 % 18:1-DAG ~80 % 18:2-DAG ~70 % 18:3-DAG	2 nmol [^{14}C]18:1/18:1-PC, 2 nmol [14C] 18:2/18:2-PC, 2 nmol [^{14}C]18:3/18:3-PC + 16 nmol 18:1/18:1-DAG	18:1/18:1-DAG, 18:2/18:2-DAG, 18:3/18:3-DAG					
	CsPDCT1	~100 %	16 nmol [^{14}C]18:1/18:1-DAG + 6 nmol 18:1/18:1-PC	PC	TLC + Radiography				
		~100 %	16 nmol [^{14}C]22:1/22:1-DAG + 6 nmol 22:1/22:1-PC						
C. sativa *R. communis*	CsPDCT1 RcROD1	100 % (42 % radioactivity) 100 % (40 % radioactivity)	12.5 nmol [^{14}C]G3P + 25 nmol 18:3-CoA	PC	TLC + Radiography	60 min 100 μg 50 μL	30 °C Tris (pH 7.2) reaction buffer	H1246 pYES-DEST52	[69]
		12 % (5 % radioactivity) 140 % (56 % radioactivity)	12.5 nmol [^{14}C]G3P + 25 nmol 18:1OH-CoA						
		10 % (4 % radioactivity) 100 % (40 % radioactivity)	12.5 nmol [^{14}C]G3P + 10 nmol 18:3-CoA, 15 nmol 18:1OH-CoA						
Oryza sativa L.	OsLP1 (Nip) OsLP1 (9311)	639 % 1819 %	2.5 nmol *sn*-1-16:0-*sn*-2-[^{14}C]18:1-PC, 100 nmol *sn*-1-16:0-*sn*-2-18:1-PC + 100 nmol 18:1/18:1-DAG	DAG	TLC + Radiography	10 min 50 μg 100 μL	30 °C MOPS (pH 7.5) reaction buffer	YNL130C pYES2	[25]

(*continued on next page*)

Table 2 (*continued*)

Species	Enzyme	Activity (nmol/mg/min), relative activity, or notes	Reaction substrates	Detected products	Detection method	Reaction time, microsome protein amount & reaction volume	Reaction temperature & buffer	*Saccharomyces cerevisiae* strains & plasmids	Ref
		100 % 100 %	2.5 nmol *sn*-1-16:0-*sn*-2-[^{14}C]16:0-PC, 100 nmol *sn*-1-16:0-*sn*-2-16:0-PC + 100 nmol 18:1/18:1-DAG						
		8 % 69 %	2.5 nmol *sn*-1-18:1-*sn*-2-[^{14}C]18:1-PC, 100 nmol 18:1/18:1-PC + 100 nmol 18:1/18:1-DAG						
	OsLP1 (Nip) OsLP1 (9311)	131 % 134 %	2.5 nmol *sn*-1-16:0-*sn*-2-[^{14}C]16:0-PC, 100 nmol 16:0/16:0-PC + 100 nmol 16:0/16:0-DAG	DAG					
		100 % 100 %	2.5 nmol *sn*-1-16:0-*sn*-2-[^{14}C]16:0-PC, 100 nmol 16:0/16:0-PC + 100 nmol 18:1/18:1-DAG						
		95 % 105 %	2.5 nmol *sn*-1-16:0-*sn*-2-[^{14}C]16:0-PC, 100 nmol 16:0/16:0-PC + 100 nmol 18:2/18:2-DAG						
	OsLP1 (Nip) OsLP1 (9311)	67 % 78 %	2.5 nmol *sn*-1-18:1-*sn*-2-[^{14}C]18:1-PC, 100 nmol 18:1/18:1-PC + 100 nmol 16:0/16:0-DAG	DAG					
		100 % 100 %	2.5 nmol *sn*-1-18:1-*sn*-2-[^{14}C]18:1-PC, 100 nmol 18:1/18:1-PC + 100 nmol 18:1/18:1-DAG						
		82 % 101 %	2.5 nmol *sn*-1-18:1-*sn*-2-[^{14}C]18:1-PC, 100 nmol 18:1/18:1-PC + 100 nmol 18:2/18:2-DAG						
Glycine max *A. thaliana*	GmPDCT1 GmPDCT2 AtROD1 GmPDCT1 1-77× GmPDCT1 D171A GmPDCT1 S184A GmPDCT1 D230A	0.15 (100 %) 0.08 (100 %) 0.22 Inactive (0%) Inactive (0 %) Inactive (2.2 %) Inactive (5.9 %)	100 nmol 18:1/18:1-DAG + 100 nmol 18:2/18:2-PC	18:2/18:2-DAG	TLC + GC-FID	120 min 100 μg 100 μL	30 °C MOPS (pH 7.5) reaction buffer	YNL130C pYES2-NTA	[29]
	GmPDCT1 GmPDCT2	50 % 40 %	100 nmol 16:0/16:0-DAG + 100 nmol 18:2/18:2-PC						

Accession numbers: AtROD1 (NP_566527), BnROD1.A3 (XP_013736317), BnROD1.C3 (XP_013702685), BnROD1.A5 (XP_013700801), BnROD1·C5 (XP_013695400), CsPDCT1 (QJD09136), GmPDCT1 (XP_003528315), GmPDCT2 (XP_003531718), HaPDCT1 (ARQ87993), LuPDCT1 (AHE80679), LuPDCT2 (AHE80680), OsLP1 (Cv.Nipponbare; XP_015644243), PiPDCT1 (XP_002899093), PiPDCT2 (XP_002907829), RcROD1 (XP_002517643).

Reaction buffer: MOPS reaction buffer contains 50 mM 3-(N-morpholino) propanesulfonic acid (MOPS)/NaOH, 20 mM $MgCl_2$, 0.45 % (*v*/v) Triton X-100; Tris reaction buffer contains 0.1 M Tris-HCl, 5 mM $MgCl_2$, 2 μg/μL of BSA.

Abbreviations: FID, flame ionizing detector; GC, gas chromatography; TLC, thin layer chromatography.

acetate incorporated approximately twice as much radioactivity into both TAG and DAG compared to wild-type plants, suggesting that enhanced PDCT activity increases flux toward TAG [21].

PDCT exhibits broad substrate specificity toward different fatty acids within both PC and DAG (Table 2) [8,9,15,20,25,29]. For instance, AtROD1 is capable of utilizing *sn*-1,2-dioleoyl-glycerol (18:1/18:1-DAG), *sn*-1,2-dioleoyl-glycero-3-phosphatidylcholine (18:1/18:1-PC) and *sn*-1,2-dimyristoyl-glycero-3-phosphatidylcholine (14:0/14:0-PC) as substrates [8]. Similarly, PDCT from camelina, sunflower, rice, and soybean can act on various DAG and PC molecules containing palmitic (16:0), 18:1, 18:2, and/or 18:3 fatty acids, although substrate preferences vary. For example, soybean PDCT1 and PDCT2 show roughly a two-fold preference for 18:1/18:1-DAG over 16:0/16:0-DAG when co-incubated with 18:2/18:2-PC [29]. Sunflower PDCT prefers 18:1/18:1-DAG over 18:2/18:2-DAG (~1.6-fold) with 18:1/18:1-PC, but favors 18:2/18:2-DAG over 18:1/18:1-DAG (~2.3-fold) with 18:1/18:2-PC [22]. Similarly, rice PDCT (OsLP1) showed slightly higher activity with 16:0/16:0-DAG than with 18:1/18:1-DAG or 18:2/18:2-DAG when incubated with 16:0/16:0-PC, but 16:0/16:0-DAG became the least active when 18:1/18:1-PC was used instead [25]. Interestingly, when swapping the reaction direction and utilizing 18:1/18:1-DAG and combinations of either 16:0/16:0-PC, 16:0/18:1-PC or 18:1/18:1-PC, there was a substantial increase (6–17 fold) in the relative activity of 16:0/16:0-PC [25]. Notably, different PDCTs exhibit varying preferences for unusual fatty acids, such as ricinoleic acid. For example, both castor PDCT (RcROD1) and AtROD1 efficiently utilize ricinoleate-PC and 18:1/18:1-DAG as substrates, although activity toward ricinoleate-PC is lower than with soy PC when incubated with 18:1/18:1-DAG, despite Arabidopsis not naturally producing ricinoleic acid [15]. In contrast, camelina PDCT is capable of utilizing 18:1/18:1-, 18:2/18:2-, and 18:3/18:3-DAG (with endogenous PC of yeast microsomes), 18:1/18:1-, 18:2/18:2-, and 18:3/18:3-PC (with 18:1/18:1-DAG) and 22:1/22:1-DAG with 22:1/22:1-PC without strong selectivity, but does not utilize ricinoleate-DAG [9,20]. In another assay incubating membranes from H1246 yeast expressing camelina or castor *PDCT* with [^{14}C]G3P and either 18:3-CoA or ricinoleoyl-CoA, camelina PDCT preferentially used 18:3-DAG but not ricinoleate-DAG, whereas castor PDCT efficiently utilized both [69]. Interestingly, castor PDCT displayed a strong preference for DAG species containing a single ricinoleoyl group at the *sn*-2 position over DAG with ricinoleate at the *sn*-1 position, as well as a > 10-fold selectivity for DAG with one ricinoleoyl group compared DAG with two ricinoleoyl groups [69]. Given that PDCT catalyzes a symmetrical interconversion between DAG and PC, most studies assessing PDCT substrate preference for unusual fatty acids examine only one direction of the reaction, leaving the full picture of PDCT specificity across both directions unresolved. A comparative analysis of PDCT substrate preference in both directions would be valuable.

Current evidence suggests that PDCT is selective for the *sn*-1,2 enantiomer of DAG and cannot utilize the *sn*-2,3 enantiomer, as the activity of camelina PDCT toward an *sn*-1,2/2,3-rac-18:1/18:1-DAG racemic mixture is approximately equivalent to that observed with half the amount of *sn*-1,2-18:1/18:1-DAG (Table 2) [9]. Additionally, despite PDCT being a homolog of SMS, it seems that PDCT is specific for PC and DAG, and cannot utilize ceramide alongside PC to generate sphingomyelin [9], nor can it transfer phosphocholine groups from either cytidine diphosphate-choline, lyso-PC, or utilize free phosphocholine directly [8]. PDCT also lacks phosphatic acid phosphatase activity [8].

6. Structural features

PDCT is predicted to be comprised of a large hydrophilic N-terminal domain, a multi-spanning, membrane embedded α-helical bundle, and a small hydrophilic C-terminal domain, with both termini oriented toward the cytoplasm (Fig. 3, Supplemental Fig. S1). In PDCT from the currently characterized species, the N-terminal region ranges from 48 to 78 amino acids, and the C-terminal region from 8 to 29 amino acids, both showing low sequence conservation (Fig. 3). The N-terminus of PDCT is predicted to be intrinsically disordered and to participate in protein-protein interactions (Supplemental Fig. S2). The membrane-embedded domain is highly conserved, consisting of eight α-helices, six of which span the membranes while the remaining two reside at the membrane-solution interface. This domain includes two motifs conserved among LPT proteins: C2 (SGH) and C3 (HXXXD) [12]. Given their substrate similarly and homology to SMS and other LPT proteins, the amino acids from these two motifs likely form a catalytic triad, comprised of the histidines from both the C2 and C3 motifs, along with the aspartic acid from the C3 motif (Fig. 3, Supplemental Fig. S3) [8,10,11,72].

Although its structure and catalytic mechanisms have not been experimentally elucidated, recent studies on PDCT sequence variations and mutagenesis have provided valuable insights into its structure-function relationships. The intrinsically disordered N-terminus of PDCT seems to play a role in enzyme function and substrate specificity, but its effects are variable and not fully consistent. In rice, allelic variation of *PDCT* sequences between two distinct cultivars *indica* (9311) and *japonica* (Nipponbare, Nip) contributed to changes in saturated TAG content [25]. The two PDCT isoforms OsLP1^{9311} and OsLP1^{Nip} only differ by two amino acids at the N-terminus (positions 40 and 43 in the PDCT consensus sequence, Fig. 3), which resulted in a preference for PC substrates with saturated fatty acids [25]. More specifically, two amino acid residue substitutions in OsROD1^{9311} (E57G and K60S) led to a 3-fold increase in its substrate preference for 16:0/16:0-PC [25]. Similarly, in canola, two PDCT isoforms, BnROD1.A3 and BnROD1.C3, differ by five amino acids within the N-terminus (positions 34, 48, and 51–53 in the consensus sequence, Fig. 3) [19]. Both isoforms encode active enzymes, which can complement the Arabidopsis *rod1* mutant to differing degrees [19]. More specifically, expression of *BnROD1.A3* complemented the lipid phenotype of *rod1* to near wild-type level by decreasing C18:1 content from ~37 % to 18 % and increasing C18:2 content from ~18 % to 33 % and C18:3 content from ~16 % to 19 %. In contrast, expression of *BnROD1.C3* in *rod1* decreased C18:1 content from ~36 % to 22 %, increased C18:2 content from ~12 % to 25 % and C18:3 content from ~12 % to 14 %, but with the line still showing a ~ 57 % relative increase in C18:1 and ~ 14 % and ~ 26 % decreases in C18:2 and C18:3, respectively, compared to the wild type [19]. Although further *in vitro* enzyme assays are needed, this suggests that BnROD1.A3 may be more active than BnROD1.C3. This difference could be attributed to amino acid substitutions in the N-terminus, potentially affecting enzyme activity, abundance, stability, localization, and/or interactions with other proteins.

The conserved transmembrane domain regions house active sites and catalytic pockets, but how these domains and specific amino acids in these regions influence PDCT activity remain less explored. Our recent mutagenesis of GmPDCT1 targeting the first transmembrane helices highlights the importance of this region for enzyme function. The removal of the first 77 amino acid residues (α1 and α2), including the first transmembrane α-helix (α2), resulted in an inactive enzyme (GmPDCT1$_{78–279}$) [29]. This region is particularly important because it may form the swapped domain that completes the catalytic pocket, as suggested by our structural analysis (see Section 7).

The influence of various amino acids within the α4 and α5 helices on enzyme activity has also been investigated by site directed mutagenesis and *in vitro* enzyme activity assay in two canola PDCT paralogs, BnROD1.A3 and BnROD1.C3 [19]. Substitutions of R146K and T150I in BnROD1.A3 (positions 150 and 154 in the PDCT consensus sequence, α4–5, both conserved, Fig. 3) significantly reduced activity to 14 % and 3 % of the wild-type protein, respectively, while G161S (positions 165 in the PDCT consensus sequence, α5, highly conserved, Fig. 3) completely abolished its activity [19]. Meanwhile, in BnROD1.C3, the R144K and T133M substitutions (positions 150 and 140 in the PDCT consensus sequence, α4–5, T140 not conserved, Fig. 3), did not alter the proteins activity, while the P170S and E142K substitutions both reduced the

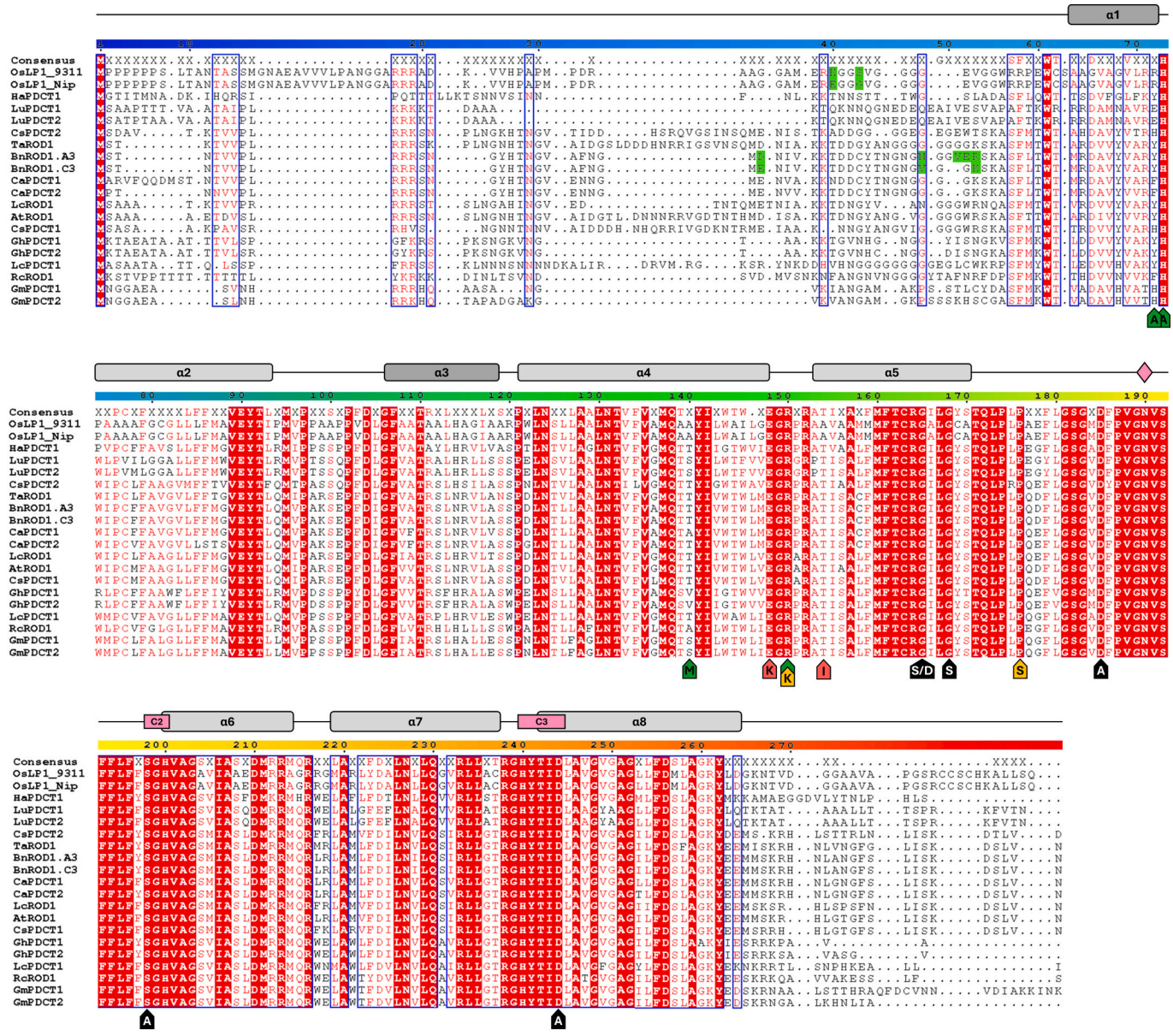

Fig. 3. Sequence alignment of characterized PDCTs. Regions corresponding to the eight α helices (transmembrane, light grey; peripheral, dark grey) that make up the structure are annotated below. The conserved motifs typical of LPT proteins, denoted C2 and C3, are highlighted in purple. Arrows and bars beneath the alignment indicate various mutagenesis experiments. Each marker lists the corresponding amino acid mutation and the colour of each marker reflects the effect of that mutation at the given position. Green ≥ 80 % activity, yellow ≥ 50 % activity, orange ≥ 10 % activity, red <10 % activity and black = loss of activity. Stacked markers indicate mutations with different reported activities. Mutation data collected from Bai et al. (2020) [19], Chen (2012) [42], and Ulch et al. (2025) [29]. The pink diamond indicates a putative N-linked glycosylation site predicted at position 190 via PTMGPT2. Regions highlighted in green represent examined polymorphisms between closely related sequences. The accession numbers of these proteins are listed in Supplemental Table S1. (For interpretation of the references to colour in this figure legend, the reader is referred to the web version of this article.)

protein activity to 15 % and 4 % of the wild-type protein, respectively (positions 176 and 148 in the PDCT consensus sequence, α4–5, both highly conserved, Fig. 3). Lastly, the G159D mutation completely abolished activity (position 165 in the PDCT consensus sequence, conserved, α5, Fig. 3) [19]. Interestingly, the R144K mutation had no effect on BnROD1.C3, while significantly affecting BnROD1.A3 (R146K), with no obvious explanation [19]. The T133M, E142K, R146K, and T150I mutations, which markedly reduce enzyme activity, are particularly interesting because they occur on the suspected cytosolic face of the protein, distant from the active site [19].

Furthermore, in another study using GmPDCT1, point mutations of three conserved amino acids within the α5–6 and α8 helices to alanine showed marked reduction in activity [29]. The three constructed mutants, D171A, S184A and D230A (positions 185, 198 and 244 in the consensus sequences, highly conserved, Fig. 3) had significantly reduced relative activities; D171A activity was lost completely, while S184A and D230A were reduced to 2.2 % and 5.9 % of wild-type GmPDCT1, respectively (Table 2). The S184A and D230A mutations reside within the C2 (α6) and C3 (α8) motif of PDCT, respectively, while D171A resides in the loop connecting α5 and α6. This loop is highly conserved among PDCT proteins and appears to form a flexible region linking the α5 and α6 transmembrane helices. Predictions using PTMGPT2 (https://nsclbio.jbnu.ac.kr/tools/ptmgpt2/; accessed 2025–11–11) have shown this region may house an N-linked glycosylation site at position 190 in the PDCT consensus sequence, with the conserved NVS motif (Fig. 3) [73]. Although not yet tested experimentally, this site could be

important for proper folding, regulation, or enzymatic activity [74]. In a separate project, an unintentional amino acid substitution of the terminal glycine within the α5 helix for serine abolished the activity of Arabidopsis ROD1 (G184S, position 168 in the consensus sequence, highly conserved, Fig. 3) [42].

7. Catalytic mechanisms

To gain further insights into the catalytic mechanism of PDCT, we predicted the AtROD1 structure using AlphaFold 3 and conducted a detailed structural analysis (Fig. 4, Supplemental Fig. S4). The model suggests a dimeric form in which the N-terminal transmembrane helix (α2) is domain-swapped, namely the helix from one protomer packs against and completes the helical bundle of the other protomer (Fig. 4A and B, Supplemental Fig. S4) [29]. Each protomer contains a helical bundle of eight α-helices (six transmembrane and two peripheral) that together form a single interior cavity. This cavity is lined by α-helices 2, 4, 5, and 6, along with the loop connecting helices 5 and 6 (Fig. 4A). The catalytic triad, composed of histidines from the C2 and C3 motifs and an aspartic acid from the C3 motif, is hypothesized to be located within this internal cavity (Fig. 3 and Fig. 4A).

As previously mentioned, PDCT is a member of the LPT family, with human SMS (hSMS) being the best studied family member [13]. In this family, the energy of the phosphoester bond of the substrate is captured by forming a covalent adduct between a nucleophilic residue in the enzyme active site and the phosphate group of the substrate. The catalytic site then requires two essential features: the nucleophile, and a general acid/base residue, which protonates the glycerol hydroxyl of the DAG leaving group (DAG product, i.e., DAG1) during PDCT cleavage of the PC substrate (PC1), and deprotonates the equivalent glycerol nucleophilic oxygen hydroxyl group of the DAG substrate (DAG2) in the product (PC2) formation step (Fig. 4). On the basis of both structures of various substrate complexes, as well as evaluating the activity of a variety of active site mutations, Hu et al. (2024) suggest that in hSMS, His301, supported by Glu205, acts as the general nucleophile, while Asp295, which forms a catalytic triad with His344 and Asp348, acts as the general acid/base [13]. Note that while this model is consistent with available mutagenesis data, it implies considerable rearrangement of the observed structures. For example, the His301 imidazole ring sits 7.5 Å from the observed bound choline phosphate position, and the environment in between is quite crowded. Since intrinsic hydrolysis prevented the key ethanolamine-linked enzyme adduct from being observed directly, this mechanism should perhaps be viewed as the currently most plausible given available data, rather than definitive.

In the active site of PDCT (AtROD1, Fig. 4), His216, His256 and Asp260 are equivalent to His301, His344 and Asp348 of hSMS, respectively [13]. There is no direct equivalent of hSMS Asp295; however, Glu105 (contributed by the C-terminal end of helix α2 of the dimeric partner, EYT motif, position 90 in the consensus sequences in Fig. 3) positions its carboxylate group in a nearly equivalent position, and moreover, forms a salt bridge with Arg180 (position 164 in the consensus sequences in Fig. 3). Arg180 in AtROD1 is equivalent to Arg243 in hSMS and adopts a near-identical conformation of the two structures. While the His256/Asp260 dyad is conserved in PDCT (positions 240 and 244 in the consensus sequences, HXXXD C3 motif, in Fig. 3), the active site tunnel is quite narrow, and since the DAG portion of PC can only fit where the tunnel widens below His216 (position 200 in the consensus sequences, SGH C2 motif, in Fig. 3), it appears that the substrate cannot easily reach deep enough into the active site to allow His256 to approach either the phosphate group or the glycerol oxygen atom. Instead, we propose that in PDCT, His256 does not act catalytically, and instead His216 acts as the nucleophile, while Glu105 acts as the general acid/base. Modeling indicates that upon PC binding, Arg180 may form a bidentate salt bridge with the substrate phosphate, while a protonated Glu105 hydrogen bonds with the glycerol O3 (Fig. 4C and D). The choline group sits in a non-polar tunnel which should interact favorably with the bulky, non-polar tertiary amine choline group, while discriminating against the smaller, and much more polar, ethanolamine primary amine. Upon attack of the phosphate by His216, Glu105 protonates O3 (Fig. 4D and E). After exchange of the DAG leaving group for a different DAG, PC is reformed by reversing this initial reaction. Testing this mechanism will be challenging, as mutations can, in addition to removing essential catalytic groups, also lead to reduced activity by destabilizing the structure. Definitively identifying the nucleophile would be extremely informative; experiments aimed at identifying the site of choline modification by mass spectrometry would perhaps be the most straightforward way of doing so.

One interesting, conserved feature of the PDCT active site is that the tunnel that accommodates the phosphocholine group is open to the ER lumen (Fig. 4). At first sight, this opening seems unnecessary: there is no net gain or loss of protons in the overall mechanism, water is not required for the mechanism (and might even lead to counterproductive hydrolysis), and the choline group cannot form hydrogen bonds with water within the tunnel, and indeed would likely be better stabilized by interactions with a non-polar tunnel roof. However, this tunnel would allow for both the priming and resetting of the acid/base histidine and the polar phosphocholine headgroup to escape should hydrolysis occurs. More subtly, and perhaps most importantly, the tunnel is likely necessary to allow water (or a small solute) to enter the active site and occupy the space left by the departing phosphocholine product. In the absence of this opening to the solvent, product release would be greatly impeded by the resulting formation of a vacuum in the active site.

8. Biotechnological applications

Bioengineering plant lipid pathways offers a powerful approach to produce oils enriched in tailored fatty acids. Given its key role in acyl editing and TAG biosynthesis, *PDCT* has been targeted in a diverse array of bioengineering strategies, including knockout, knockdown, overexpression, or combinations with other genes, primarily to modify seed lipid composition in oilseeds and other plants (Table 1).

PDCT downregulation has been commonly used to promote seed MUFA content, most notably C18:1 and C22:1, at the expense of PUFAs. To date, *PDCT* knockout and knockdown mutants of the model plant Arabidopsis, oilseeds, and several crop species have been developed through the chemical mutagen ethyl methanesulfonate (EMS), transfer DNA (T-DNA) insertional mutagenesis, RNA interference (RNAi), and clustered regularly interspaced short palindromic repeats–CRISPR associated protein 9 (CRISPR-Cas9) genome editing (Table 1). Downregulating *PDCT* increased seed C18:1 content in Arabidopsis from 15.1 % to 32.8 % [8], crambe (*C. abyssinica*) from 14 % to 18 % [17], canola (*B. napus*) from 61 % to 68 % [19], pennycress (*T. arvense* L.) from 10 % to 22 % [23,24], field cress (*L. campestre*) from 13 % to 22 % [27], soybean (*G.* max L.) from 16 % to 45 % [28], cotton (*G. hirsutum* L.) from 14.5 % to 16.5 % [31] and rice (*O. sativa* L.) from 32 % to 36 % [26,56]. These results suggest that PDCT downregulation can substantially elevate seed C18:1 in some species, such as Arabidopsis and soybean, but has only modest effects in others. This variation likely reflects differences in the relative contribution of PDCT to acyl editing among plant species even though some of them are closely related (e.g., Arabidopsis vs canola). Indeed, different species may employ distinct acyl editing and/or TAG remodeling pathways, which could mask the effects of *PDCT* loss. TAG remodeling was recently identified in *Physaria fendleri* as a key mechanism enabling the high-level accumulation of lesquerolic

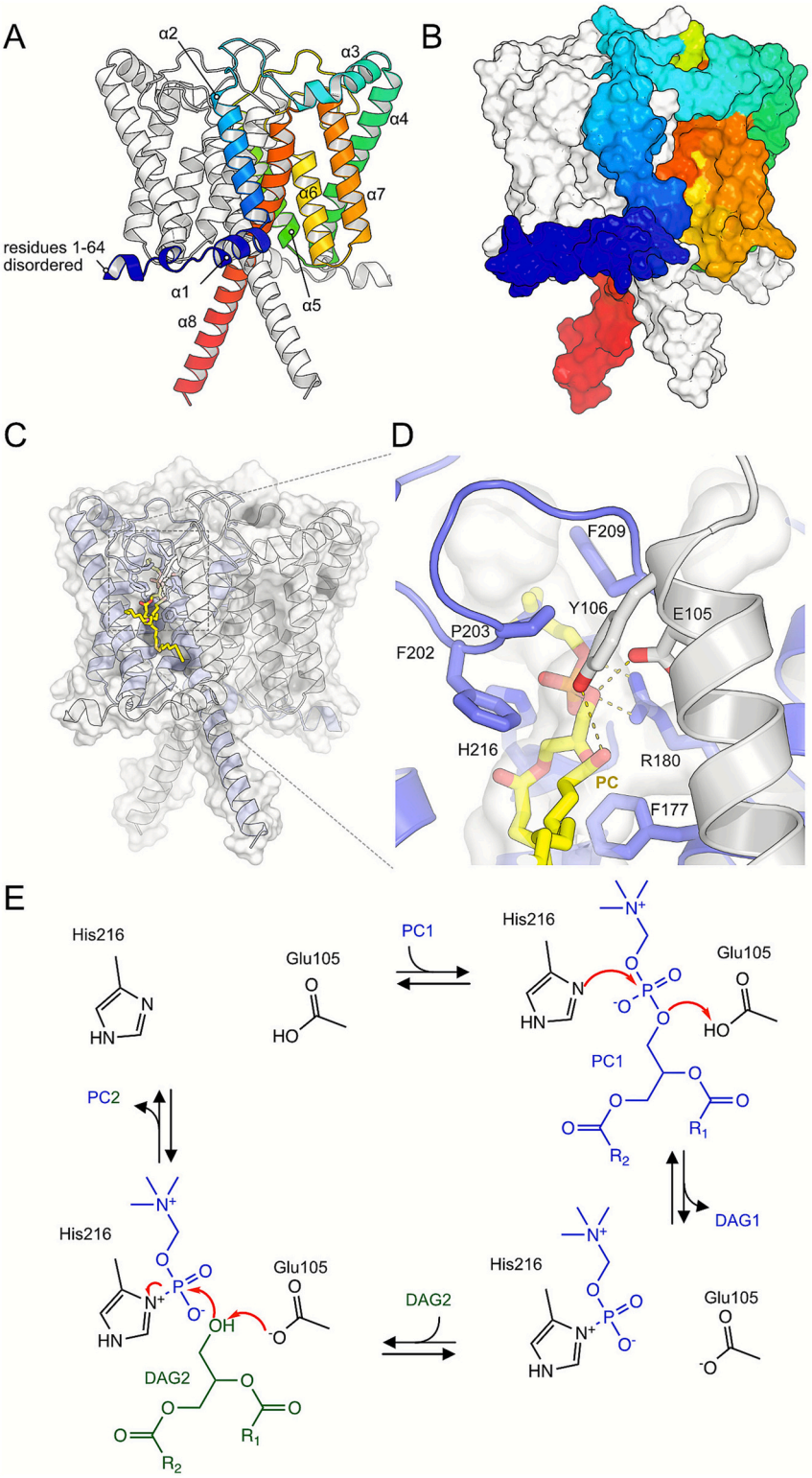

Fig. 4. Substrate binding and mechanism of PDCT. Arabidopsis PDCT (AtROD1) shown as a cartoon (A) and as a surface (B). Note that α2 from the N-terminus of one protomer completes the active site of its binding partner. Both N- and C-termini face the cytosol. A hypothetical membrane orientation of AtROD1 is shown in Supplemental Fig. S4. (C) Model of AtROD1 with PC (yellow) modelled within the active site. PC enters the active site through a tunnel that begins close to the middle of the membrane. (D) The detailed interactions between PC and the AtROD1 active site. The internal pocket of AtROD1 is shown as a semi-transparent surface. (E) Proposed mechanism of PDCT. His216 is proposed to act as the nucleophile, attacking the phosphate group of PC to form a phosphoester bond. Glu105 is proposed to act as a general acid in this step, protonating the glycerol oxygen atom of the DAG leaving group. After exchange of DAG molecules, the reaction proceeds in reverse. (For interpretation of the references to colour in this figure legend, the reader is referred to the web version of this article.)

acid (14-hydroxy-20:1$^{\Delta 11cis}$), and has been proposed to occur in other species as well [75,76]. This process involves partial TAG hydrolysis where lipases remove the *sn*-1 or 3 fatty acids to generate *sn*-1,2 or *sn*-2,3-DAG, followed by TAG resynthesis using different acyl-CoA substrates, thereby generating new TAG molecular species [77].

To further enhance seed MUFA content, *PDCT* manipulation has been combined with other genes, such as *LPCAT* and *FAE1*. Knockout of *PDCT* in combination with *LPCAT1* and *LPCAT2* in Arabidopsis further increased C18:1 content to 42.4 % and C20:1 from 19.9 % (wild-type level) to 26.1 % [55]. Similarly, RNAi-mediated downregulation of *PDCT* together with *LPCAT1–1* and *LPCAT1–2* in *C. abyssinica* increased C18:1 to 22 % and C20:1 from 1 % to 8 %, while reducing C22:1 from 60 % to 48 %, which reflects a combination of the effects seen in single-gene manipulations, where downregulation of *PDCT* resulted in an increase in C18:1 and downregulation of *LPCAT* led to an increase in C20:1 accompanied with a decrease C22:1 [17]. Furthermore, downregulation of *PDCT* together with *FAE1* in pennycress further increased C18:1 to 61 % while basically eliminating long chain fatty acids (i.e., C20:1, C22:1 and C24:1) [23,24].

Conversely, *PDCT* overexpression has been applied in plants and yeast to enhance PUFA accumulation, but with limited success. For example, overexpression of flax *PDCT* in Arabidopsis seeds and co-expression of flax *PDCT* in combination with flax *FAD2* and *FAD3* in yeast increased C18:2 from 26.9 % to 29.1 % and from 0 % to 4.6 %, respectively, and C18:3 from 16.3 % to 22.5 % and from 0 % to 6.6 % [16]. Similarly, overexpression of rice *PDCT* (*OsLIN6*) modestly increased C18:2 content in rice grains from 11 to 13 mg/g dry weight [26] and overexpression of camelina *PDCT* slightly increased C18:3 in camelina seeds from 36 to 37 % [21].

PDCT has also been used in combination with other genes to promote the accumulation of unusual fatty acids and oils with unique stereoisomeric structures. In multi-gene approaches, *PDCT* overexpression has successfully enhanced the accumulation of hydroxy, cyclic, conjugated, and epoxy fatty acids (Table 1). For example, the seed-specific co-overexpression of lychee (*L. chinensis*) *PDCT* with *Escherichia coli Cyclopropane Fatty Acid Synthase* (*EcCPS*) in camelina *fad2/fae1* mutant slightly increased the cyclic fatty acid content from 4.2 % to 5.8 % in seed oil compared to expression of *EcCPS* alone [18]. In an approach aimed at accumulating hydroxy fatty acids in Arabidopsis seeds, seed-specific overexpression of castor *ROD1* and *fatty acid hydroxylase 12* (*RcFAH12*) in wild-type and *rod1* Arabidopsis enhanced the hydroxy fatty acid content in total seed lipids from 9.9 % to 19.9 % and from 5.5 % to 9.7 % compared to overexpression of *RcFAH12* alone in the corresponding backgrounds, respectively [15]. In engineering hydroxy fatty acid accumulation in Arabidopsis, the flux of hydroxy fatty acids from DAG to PC represents a bottleneck that limits the synthesis of di- or tri-hydroxy fatty acid-TAGs [78]. This is because Arabidopsis predominately uses PC-derived DAG for TAG biosynthesis and *RcFAH12* introduces hydroxyl groups at the *sn*-2 position of PC, resulting in accumulation of *sn*-2-hydroxy fatty acid-TAG [78]. Considering AtROD1 can use ricinoleate-PC *in vitro* [15], the higher hydroxy fatty acid content observed when *RcFAH12* is expressed in wild-type Arabidopsis compared with the *rod1* mutant may reflect the ability of endogenous AtROD1 to transfer *sn*-2-ricinoleate-PC into DAG for TAG synthesis, which is lost in *rod1*. The further increase in hydroxy fatty acid content upon co-expression of castor *ROD1* is possibly due to the castor ROD1's enhanced ability to use ricinoleate-DAG relative to AtROD1 [69], although the activity of AtROD1 toward ricinoleate-DAG lacks experimental confirmation. Further increases in hydroxy fatty acid accumulation can be obtained by co-expressing *DGAT* and *Phosphatidylcholine: Diacylglycerol Acyltransferase* (*PDAT*), encoding enzymes that direct ricinoleate-DAG and PC toward TAG synthesis. Indeed, further co-expression of *RcFAH12* and *RcROD1* with *RcDGAT2* in *fae1* Arabidopsis increased hydroxy fatty acid accumulation to 28.5 % [15]. This is consistent with another report, in which co-expression of *RcFAH12*, *RcROD1*, *RcDGAT2*, *RcDGAT1–2*, and *RcLPCAT* in *fae1* Arabidopsis resulted in 27.6–28.9 % hydroxy fatty acid accumulation [79].

Production of unusual fatty acids has also been explored in other systems, including plant leaves and yeast. Epoxy fatty acids have been produced in *N. benthamiana* leaves by co-expressing *Vernonia galamensis PDCT* with a FAD2-like enzyme; however, this slightly reduced epoxy fatty acid content from 8.6 % to 8.2 % compared with expression of *VgFAD2*-like alone [80]. In *S. cerevisiae* yeast, co-expression of pomegranate (*Punica granatum*) *Fatty Acid Desaturase X* (*FADX*), *PDAT* and *PDCT* on plasmids, together with C18:2 feeding, produced 3.3 % punicic acid [81]. Remarkably, punicic acid accumulation increased to 26.7 % when a multi-gene set including *PgFADX*, *PgFAD2*, *PgPDCT*, *PgLPCAT*, *PgDGAT2* and *Rattus norvegicus FAE (ELO2)* was integrated into the yeast genome using CRISPR/Cas9-assisted Ty retrotransposon-targeted random gene shuffling [82].

In another study aimed at producing stereoisomeric lipids in Arabidopsis to mimic human milk fat, which is enriched in C16:0 at the *sn*-2 position of the glycerol backbone, *ROD1* knockout was combined with overexpression of chloroplast-localized Arabidopsis *Lysophosphatidic Acid Acyltransferase* lacking its putative chloroplast transit peptide (*AtLPAT ΔCTP*) [83]. This strategy redirected an LPAT with C16:0 substrate preference to the ER, enhancing incorporation of C16:0 over C18 fatty acids at the *sn*-2 position of TAG in seed oil. The lack of functional PDCT reduced channeling through acyl-edited PC for conversion into DAG, increasing the distribution of C16:0 at the *sn*-2 position of TAG relative to the *sn*-1 and *sn*-3 positions by 26 % (from 30 % to 56 %) compared to expression of *AtLPAT ΔCTP* alone in wild-type plants. This ratio was further increased to 71 % when further combined with silencing of endogenous *LPCAT2/3* [83].

Notably, in most bioengineering efforts, *PDCT* manipulation does not negatively affect overall plant (or yeast) fitness. Traits such as root establishment, plant vigor, flowering time, seedling weight, seed oil content, protein content, glucosinolate content, and germination rate remain comparable to wild-type controls [19,24,57]. However, as mentioned previously (see Section 3), there are several exceptions where *PDCT* loss-of-function or overexpression impacts plant performance. For example, *rod1* rice mutants exhibit altered grain epidermal morphology, reduced grain size and weight, and increased total fatty acid content [56], whereas overexpression of *CsPDCT* in camelina seeds enhances seed oil content, overall seed yield, and silique and seed number per plant [21]. Furthermore, when *PDCT* manipulation is combined with other genes to improve modified fatty acids content or generate stereoisomeric oils, negative effects on seed oil accumulation and germination can often occur, which are likely caused by the presence of the produced unique lipids themselves while PDCT often helps to mitigate such penalties (Table 1). For example, expression of *RcFAH12* in *rod1* and *fae1* Arabidopsis backgrounds reduced seed oil content by ~38 % and 40 % compared to wild type, which was alleviated to 12 % and 27 % respectively when *RcROD1* was co-expressed [15]. Seed oil content was restored to wild-type level when *RcDGAT2* was co-expressed in the *fae1* background or when *RcFAH12* was expressed with endogenous *AtROD1*. Similarly, in cyclic fatty acid production, co-expression of *LcPDCT* with *EcCPS* slightly increased seed weight, whereas expression of *EcCPS* alone reduced seed weight compared to the *fad2/fae1* camelina background [18]. These observations are consistent with the concept that, in unusual fatty acid engineering, flux through PC can create a bottleneck that inhibits acetyl-CoA carboxylase activity and reduces overall fatty acid biosynthesis [84]. A similar PC bottleneck may occur with these examples, which could be alleviated by introducing an unusual fatty acid-selective PDCT.

Beyond oil production, *PDCT* knockout has also been found to improve cotton fiber quality, where CRISPR/Cas9-mediated disruption of *PDCT1* in *G. hirsutum* (cv. Jimian14) enhanced fiber fineness, length, and strength [30].

9. Concluding remarks

PDCT is one of the recently identified enzymes involved in PC and DAG conversion and plays an important role in plant oil biosynthesis. Since the discovery of *PDCT* (*ROD1*) in Arabidopsis [8], significant progress has been made in understanding its physiological roles across species and in exploring its biotechnological potential. Numerous studies have exploited PDCT to develop plants and microorganisms that produce oils with improved properties for industrial purposes and human nutrition. Although *PDCT* knockout results in a less pronounced increase in MUFA content compared to *FAD2* knockout, which often leads to adverse physiological effects on growth and development, particularly at low temperatures [24,85,86], it does not cause major morphological defects, making *PDCT* an especially attractive target. This has driven efforts to use CRISPR-based genome editing to generate high-oleic, non-GMO germplasms with industrial value. Furthermore, PDCT editing in combination with other genes has shown promise for producing a variety of high-value lipids.

Despite recent advances, much remains unknown about PDCT, including its evolution, physiological roles beyond oil biosynthesis, regulatory mechanisms, catalytic features and structural properties. PDCT is exclusively found in higher plants and is absent in animals, wherein its closest homolog is SMS. This highlights the existence of two essential lipid pathways that are parallel in plants and animals: in plants, PDCT catalyzes the interconversion between DAG and PC by generating modified DAG from PC for TAG biosynthesis and producing new PC for further fatty acid modification, whereas in animals, SMS catalyzes the conversion between ceramide and PC generating sphingomyelin for sphingolipid biosynthesis while recycling PC and producing DAG for other lipid pathways. PDCT-like homologs may be present in some early-diverging green lineage species (i.e., nonflowering plants), whereas algae contain proteins more similar to animal SMS and SMS-like proteins rather than to higher-plant PDCTs. Although their functional characterization is still needed to determine whether they possess PDCT activity, these homologs may provide insights into the evolutionary origin of PDCT from ancestral members of the LPT protein family.

While PDCT has a major role in seed oil biosynthesis, its broader expression across plant tissues hints on additional functions, including possible roles in stress responses, that remain to be investigated. Regulation of PDCT is still poorly understood; several transcription factors have been implicated in controlling its expression, but post-translational regulation has not been explored, even though a potential glycosylation site has been predicted. PDCT has been shown to physically interact with other lipid enzymes, leading to the hypothesis that it participates in more general lipid biosynthesis interactomes and/or metabolons. Mounting evidence suggests that many ER-localized enzymes for plant lipid biosynthesis, including PDCT, can form protein complexes and/or metabolons that help channel substrates and regulate metabolic flux at pathway branch points [3,77,87–89]. Since many plant species rely heavily on flux through PC-derived DAG for TAG biosynthesis, whereas animals primarily use *de novo* DAG via the Kennedy pathway, the presence of PDCT and its participation in ER lipid biosynthetic interactomes and/or metabolons support the key role of PC as a "DAG carrier" for plant oil production [77,89]. However, the composition, dynamics, and functional significance of these putative complexes remain unclear (for reviews, see [3,87]). Furthering the understanding of the transcriptional and post-translational regulation of PDCT may help identify allied targets for manipulating TAG profiles during oil biosynthesis.

In vitro enzyme assays suggests that PDCT from certain plant species may have different substrate specificities. However, these assays were performed using yeast microsomal fractions containing recombinant PDCT rather than purified enzymes. Yeast microsomes are rich in PC and also contain small amounts of DAG [9], with acyl composition that differ from those of native plant membranes where PDCT is normally embedded. Thus, it remains unclear whether and how such differences in membrane environment (lipid composition and distribution and other embedded proteins) influence PDCT activity and substrate specificity. Future studies using purified enzymes and reconstituted membranes that better mimic native systems may be helpful in clarifying these effects and advancing our understanding of PDCT function(s) across species.

Several studies have identified residues that influence PDCT activity and function, yet the structure of PDCT itself remains to be determined. Our structural analysis (Fig. 4) suggests that PDCT may form a dimer through an N-terminal domain swapping mechanism. Considering multiple PDCT isoforms exist in various plant species, whether these proteins form homo- and/or heterodimers and whether such dimerization regulates catalytic activity remains an open question. Based on the AlphaFold3 predicted structure, we have proposed a potential catalytic mechanism of AtROD1 involving essential residues in the swapped N-terminal domain and the catalytic triad in the helix core, but further structural studies are needed to prove this mechanism. Substrate specificities of PDCT also vary among species; for example, castor PDCT prefers hydroxylated DAG species, whereas camelina PDCT cannot use these substrates [20,69], though structural explanations for these differences remain elusive. Furthermore, the large N-terminal intrinsically disordered region of PDCT is poorly conserved and predicted to lack a defined structure. While apparently less important for catalysis, it may contribute to substrate specificity, regulatory functions or mediate protein-protein interactions. Future studies addressing these and other evolutionary, regulatory, and structural aspects of PDCT will deepen our understanding of lipid metabolism and open new avenues for bioengineering plant oils.

Declaration of generative AI and AI-assisted technologies in the manuscript preparation process

During the preparation of this work the author(s) used ChatGPT in order to proofread some of the writing. After using this tool/service, the author(s) reviewed and edited the content as needed and take(s) full responsibility for the content of the published article.

CRediT authorship contribution statement

Brandon A. Ulch: Writing – review & editing, Writing – original draft, Visualization, Methodology, Formal analysis, Data curation. **Alyssa C. Clews:** Writing – review & editing, Writing – original draft, Visualization, Data curation. **Caroline A. Reisiger:** Writing – review & editing, Writing – original draft, Visualization, Data curation. **Li-Hua Zhu:** Writing – review & editing. **Robert T. Mullen:** Writing – review & editing. **Matthew S. Kimber:** Writing – review & editing, Writing – original draft, Visualization, Software, Methodology, Formal analysis, Data curation. **Yang Xu:** Writing – review & editing, Writing – original draft, Visualization, Supervision, Funding acquisition, Formal analysis, Data curation, Conceptualization.

Funding

Support for this work was provided by the University of Guelph Start-up Research Grant (YX), Natural Sciences and Engineering Research Council of Canada Discovery Grant (RGPIN-2022-03459, YX; RGPIN-2020-07113, MSK; RGPIN-2018-04629, RTM), the Ontario Agri-Food Innovation Alliance Grant (UG-T1-2023-102164, YX), and Trees and Crops for the Future (TC4F) SLU Strategic Research Environment (LHZ). ACC and CAR are recipients of Ontario Graduate Scholarships.

Declaration of competing interest

The authors declare no conflict of interest.

Appendix A. Supplementary data

Supplementary data to this article can be found online at https://doi.org/10.1016/j.plipres.2025.101361.

Data availability

Data will be made available on request.

References

[1] Biermann U, Bornscheuer UT, Feussner I, Meier MA, Metzger JO. Fatty acids and their derivatives as renewable platform molecules for the chemical industry. Angew Chem Int Ed 2021;60:20144–65. https://doi.org/10.1002/anie.202100778.

[2] Xu Q, Tang Q, Xu Y, Wu J, Mao X, Li F, et al. Biotechnology in future food lipids: opportunities and challenges. Annu Rev Food Sci Technol 2023;14:225–46. https://doi.org/10.1146/annurev-food-060721-024353.

[3] Clews AC, Ulch BA, Jesionowska M, Hong J, Mullen RT, Xu Y. Variety of plant oils: species-specific lipid biosynthesis. Plant Cell Physiol 2024;65:845–62. https://doi.org/10.1093/pcp/pcad147.

[4] Hildebrand DF, Adams TR, Dahmer ML, Williams EG, Collins GB. Analysis of lipid composition and morphological characteristics in soybean regenerants. Plant Cell Rep 1989;7:701–3. https://doi.org/10.1007/BF00272065.

[5] Ruiz-Gutiérrez V, Pérez-Espinosa A, Vázquez CM, Santa-María C. Effects of dietary fats (fish, olive and high-oleic-acid sunflower oils) on lipid composition and antioxidant enzymes in rat liver. Br J Nutr 1999;82:233–41. https://doi.org/10.1017/S0007114599001415.

[6] Ogunniyi D. Castor oil: a vital industrial raw material. Bioresour Technol 2006;97:1086–91. https://doi.org/10.1016/j.biortech.2005.03.028.

[7] Mutlu H, Meier MAR. Castor oil as a renewable resource for the chemical industry. Eur J Lipid Sci Technol 2010;112:10–30. https://doi.org/10.1002/ejlt.200900138.

[8] Lu C, Xin Z, Ren Z, Miquel M, Browse J. An enzyme regulating triacylglycerol composition is encoded by the *ROD1* gene of Arabidopsis. Proc Natl Acad Sci 2009;106:18837–42. https://doi.org/10.1073/pnas.0908848106.

[9] Demski K, Jeppson S, Stymne S, Lager I. *Camelina sativa* phosphatidylcholine: diacylglycerol cholinephosphotransferase-catalyzed interconversion does not discriminate between substrates. Lipids 2021;56:591–602. https://doi.org/10.1002/lipd.12322.

[10] Wang P, Chen Z, Kasimu R, Chen Y, Zhang X, Gai J. Genome-wide analysis suggests divergent evolution of lipid. Genome 2016;59:589–601. https://doi.org/10.1139/gen-2016-0061.

[11] Tong S, Lin Y, Lu S, Wang M, Bogdanov M, Zheng L. Structural insight into substrate selection and catalysis of lipid phosphate phosphatase PgpB in the cell membrane. J Biol Chem 2016;291:18342–52. https://doi.org/10.1074/jbc.M116.737874.

[12] Sigal YJ, McDermott MI, Morris AJ. Integral membrane lipid phosphatases/phosphotransferases: common structure and diverse functions. Biochem J 2005;387:281–93. https://doi.org/10.1042/BJ20041771.

[13] Hu K, Zhang Q, Chen Y, Yang J, Xia Y, Rao B, et al. Cryo-EM structure of human sphingomyelin synthase and its mechanistic implications for sphingomyelin synthesis. Nat Struct Mol Biol 2024;31:884–95. https://doi.org/10.1038/s41594-024-01237-2.

[14] Lemieux B, Miquel M, Somerville C, Browse J. Mutants of Arabidopsis with alterations in seed lipid fatty acid composition. Theor Appl Genet 1990;80:234–40. https://doi.org/10.1007/BF00224392.

[15] Hu Z, Ren Z, Lu C. The phosphatidylcholine diacylglycerol cholinephosphotransferase is required for efficient hydroxy fatty acid accumulation in transgenic arabidopsis. Plant Physiol 2012;158:1944–54. https://doi.org/10.1104/pp.111.192153.

[16] Wickramarathna AD, Siloto RMP, Mietkiewska E, Singer SD, Pan X, Weselake RJ. Heterologous expression of flax Phospholipid:Diacylglycerol Cholinephosphotransferase (PDCT) increases polyunsaturated fatty acid content in yeast and Arabidopsis seeds. BMC Biotechnol 2015;15:63. https://doi.org/10.1186/s12896-015-0156-6.

[17] Guan R, Li X, Hofvander P, Zhou X, Wang D, Stymne S, et al. RNAi targeting putative genes in phosphatidylcholine turnover results in significant change in fatty acid composition in *Crambe abyssinica* seed oil. Lipids 2015;50:407–16. https://doi.org/10.1007/s11745-015-4004-1.

[18] Yu X-H, Cai Y, Chai J, Schwender J, Shanklin J. Expression of a lychee *PHOSPHATIDYLCHOLINE: DIACYLGLYCEROL CHOLINEPHOSPHOTRANSFERASE* with an *Escherichia coli CYCLOPROPANE SYNTHASE* enhances cyclopropane fatty acid accumulation in camelina seeds. Plant Physiol 2019;180:1351–61. https://doi.org/10.1104/pp.19.00396.

[19] Bai S, Wallis JG, Denolf P, Engelen S, Bengtsson JD, Van Thournout M, et al. The biochemistry of headgroup exchange during triacylglycerol synthesis in canola. Plant J 2020;103:83–94. https://doi.org/10.1111/tpj.14709.

[20] Lager I, Jeppson S, Gippert A-L, Feussner I, Stymne S, Marmon S. Acyltransferases regulate oil quality in *Camelina sativa* through both acyl donor and acyl acceptor specificities. Front Plant Sci 2020;11:1144. https://doi.org/10.3389/fpls.2020.01144.

[21] Abdullah HM, Pang N, Chilcoat B, Shachar-Hill Y, Schnell DJ, Dhankher OP. Overexpression of the *phosphatidylcholine: diacylglycerol Cholinephosphotransferase (PDCT)* gene increases carbon flux toward triacylglycerol (TAG) synthesis in *Camelina sativa* seeds. Plant Physiol Biochem 2024;208:108470. https://doi.org/10.1016/j.plaphy.2024.108470.

[22] Mapelli Brahm A. Estudio de enzimas implicadas en el intercambio de acilos y la síntesis de glicerolípidos en el retículo endoplásmico de girasol (*Helianthus annuus*). Doctoral dissertation. Universidad de Sevilla; 2020. https://hdl.handle.net/11441/98220.

[23] Chopra R, Johnson EB, Emenecker R, Cahoon EB, Lyons J, Kliebenstein DJ, et al. Identification and stacking of crucial traits required for the domestication of pennycress. Nat Food 2020;1:84–91. https://doi.org/10.1038/s43016-019-0007-z.

[24] Jarvis BA, Romsdahl TB, Mcginn MG, Nazarenus TJ, Cahoon EB, Chapman KD, et al. CRISPR/Cas9-induced *fad2* and *rod1* mutations stacked with *fae1* confer high oleic acid seed oil in pennycress (*Thlaspi arvense* L.). Frontiers. Plant Sci 2021;12:652319. https://doi.org/10.3389/fpls.2021.652319.

[25] Hong J, Rosental L, Xu Y, Xu D, Orf I, Wang W, et al. Genetic architecture of seed glycerolipids in Asian cultivated rice. Plant Cell Environ 2023;46:1278–94. https://doi.org/10.1111/pce.14378.

[26] Zhou H, Xia D, Li P, Ao Y, Xu X, Wan S, et al. Genetic architecture and key genes controlling the diversity of oil composition in rice grains. Mol Plant 2021;14:456–69. https://doi.org/10.1016/j.molp.2020.12.001.

[27] Sandgrind S, Li X, Ivarson E, Wang ES, Guan R, Kanagarajan S, et al. Improved fatty acid composition of field cress (*Lepidium campestre*) by CRISPR/Cas9-mediated genome editing. Front Plant Sci 2023;14:1076704. https://doi.org/10.3389/fpls.2023.1076704.

[28] Li H, Zhou R, Liu P, Yang M, Xin D, Liu C, et al. Design of high-monounsaturated fatty acid soybean seed oil using *GmPDCTs* knockout via a CRISPR-Cas9 system. Plant Biotechnol J 2023;21:1317–9. https://doi.org/10.1111/pbi.14060.

[29] Ulch BA, Clews AC, Jesionowska MW, Kimber MS, Mullen RT, Xu Y. Characterization of phosphatidylcholine:diacylglycerol cholinephosphotransferases from soybean (*Glycine max*). J Agric Food Chem 2025;73:7645–57. https://doi.org/10.1021/acs.jafc.4c12704.

[30] Ding B, Liu B, Zhu X, Zhang H, Hu R, Li S, et al. Downregulation of the *GhROD1* gene improves cotton fiber fineness by decreasing acyl pool saturation, stimulating small heat shock proteins (sHSPs), and reducing H2O2 production. IJMS 2024;25:11242. https://doi.org/10.3390/ijms252011242.

[31] Li T, Long L, Tang Y, Xu Z, Wang G, Jiang M, et al. Knock-out of *GhPDCT* with the CRISPR/Cas9 system increases the oleic acid content in cottonseed oil. J Integr Agric 2024;23:3468–71. https://doi.org/10.1016/j.jia.2024.07.030.

[32] Ran X, Hong J, Yan F, Shi J. Identification and bioinformatics analysis on phosphatidylcholine diglyceride choline phosphotransferase family genes in plants. Plant Gene Trait 2023;14:1–10. https://doi.org/10.5376/pgt.2023.14.0003.

[33] Zhao X, Dauenpen M, Qu C, Qiu X. Genomic analysis of genes involved in the biosynthesis of very long chain polyunsaturated fatty acids in *Thraustochytrium* sp. 26185. Lipids 2016;51:1065–75. https://doi.org/10.1007/s11745-016-4181-6.

[34] Yue X-H, Chen W-C, Wang Z-M, Liu P-Y, Li X-Y, Lin C-B, et al. Lipid distribution pattern and transcriptomic insights revealed the potential mechanism of docosahexaenoic acid traffics in *Schizochytrium* sp. A-2. J Agric Food Chem 2019;67:9683–93. https://doi.org/10.1021/acs.jafc.9b03536.

[35] Yang P, Li X, Shipp MJ, Shockey JM, Cahoon EB. Mining the bitter melon (*Momordica charantia* l.) seed transcriptome by 454 analysis of non-normalized and normalized cDNA populations for conjugated fatty acid metabolism-related genes. BMC Plant Biol 2010;10:250. https://doi.org/10.1186/1471-2229-10-250.

[36] Cui P, Lin Q, Fang D, Zhang L, Li R, Cheng J, et al. Tung tree (*Vernicia fordii*, Hemsl.) genome and transcriptome sequencing reveals co-ordinate up-regulation of fatty acid β-oxidation and triacylglycerol biosynthesis pathways during eleostearic acid accumulation in seeds. Plant Cell Physiol 2018;59:1990–2003. https://doi.org/10.1093/pcp/pcy117.

[37] Geiger O, López-Lara IM, Sohlenkamp C. Phosphatidylcholine biosynthesis and function in bacteria. Biochim Biophys Acta (BBA) Mol Cell Biol Lipids 2013;1831:503–13. https://doi.org/10.1016/j.bbalip.2012.08.009.

[38] Güler S, Seeliger A, Härtel H, Renger G, Benning C. A null mutant of Synechococcus sp. PCC7942 deficient in the sulfolipid sulfoquinovosyl diacylglycerol. J Biol Chem 1996;271:7501–7. https://doi.org/10.1074/jbc.271.13.7501.

[39] Harwood JL, Guschina IA. The versatility of algae and their lipid metabolism. Biochimie 2009;91:679–84. https://doi.org/10.1016/j.biochi.2008.11.004.

[40] Xu Y. Biochemistry and biotechnology of lipid accumulation in the microalga *Nannochloropsis oceanica*. J Agric Food Chem 2022;70:11500–9. https://doi.org/10.1021/acs.jafc.2c05309.

[41] Boratyn GM, Schäffer AA, Agarwala R, Altschul SF, Lipman DJ, Madden TL. Domain enhanced lookup time accelerated BLAST. Biol Direct 2012;7:12. https://doi.org/10.1186/1745-6150-7-12.

[42] Chen Y. Molecular analysis of genes involved in the biosynthesis of very long chain polyunsaturated fatty acids (VLCPUFAs). Master's thesis. University of Saskatchewan; 2012. http://hdl.handle.net/10388/ETD-2012-06-520.

[43] Schmid M, Davison TS, Henz SR, Pape UJ, Demar M, Vingron M, et al. A gene expression map of *Arabidopsis thaliana* development. Nat Genet 2005;37:501–6. https://doi.org/10.1038/ng1543.

[44] Kim HU, Chen GQ. Identification of hydroxy fatty acid and triacylglycerol metabolism-related genes in lesquerella through seed transcriptome analysis. BMC Genomics 2015;16:230. https://doi.org/10.1186/s12864-015-1413-8.

[45] Kim HU, Lee K-R, Shim D, Lee JH, Chen GQ, Hwang S, et al. Transcriptome analysis and identification of genes associated with ω-3 fatty acid biosynthesis in *Perilla frutescens* (L.) var. frutescens. BMC Genomics 2016;17:474. https://doi.org/10.1186/s12864-016-2805-0.

[46] Hu X-D, Pan B-Z, Fu Q, Niu L, Chen M-S, Xu Z-F. *De novo* transcriptome assembly of the eight major organs of Sacha Inchi (*Plukenetia volubilis*) and the identification of

genes involved in α-linolenic acid metabolism. BMC Genomics 2018;19:380. https://doi.org/10.1186/s12864-018-4774-y.
[47] Saini R, Kumar S. Genome-wide identification, characterization and *in-silico* profiling of genes encoding FAD (fatty acid desaturase) proteins in chickpea (*Cicer arietinum* L.). Plant. Gene 2019;18:100180. https://doi.org/10.1016/j.plgene.2019.100180.
[48] Wang L, Zhang Y, Li D, Dossa K, Wang ML, Zhou R, et al. Gene expression profiles that shape high and low oil content sesames. BMC Genet 2019;20:45. https://doi.org/10.1186/s12863-019-0747-7.
[49] Zhang G, Bahn SC, Wang G, Zhang Y, Chen B, Zhang Y, et al. *PLDα1*-knockdown soybean seeds display higher unsaturated glycerolipid contents and seed vigor in high temperature and humidity environments. Biotechnol Biofuels 2019;12:9. https://doi.org/10.1186/s13068-018-1340-4.
[50] Claver A, Luján MÁ, Escuín JM, Schilling M, Jouhet J, Savirón M, et al. Transcriptomic and lipidomic analysis of the differential pathway contribution to the incorporation of erucic acid to triacylglycerol during pennycress seed maturation. Front. Plant Sci 2024:15. https://doi.org/10.3389/fpls.2024.1386023.
[51] Parchuri P, Pappanoor A, Naeem A, Durrett TP, Welti R, Sreedhar R. Lipidome analysis and characterization of *Buglossoides arvensis* acyltransferases that incorporate polyunsaturated fatty acids into triacylglycerols. Plant Sci 2022;324:111445. https://doi.org/10.1016/j.plantsci.2022.111445.
[52] Shi W, Zhang D, Ma Z. Transcriptome analysis of genes involved in fatty acid and lipid biosynthesis in developing walnut (*Juglans regia* L.) seed kernels from Qinghai plateau. Plants 2022;11:3207. https://doi.org/10.3390/plants11233207.
[53] Niu J, Chen Y, An J, Hou X, Cai J, Wang J, et al. Integrated transcriptome sequencing and dynamic analysis reveal carbon source partitioning between terpenoid and oil accumulation in developing *Lindera glauca* fruits. Sci Rep 2015;5:15017. https://doi.org/10.1038/srep15017.
[54] Mai Y, Huo K, Yu H, Zhou N, Shui L, Liu Y, et al. Using lipidomics to reveal details of lipid accumulation in developing Siberian apricot (*Prunus sibirica* L.) seed kernels. GCB Bioenergy 2020;12:539–52. https://doi.org/10.1111/gcbb.12693.
[55] Bates PD, Fatihi A, Snapp AR, Carlsson AS, Browse J, Lu C. Acyl editing and headgroup exchange are the major mechanisms that direct polyunsaturated fatty acid flux into triacylglycerols. Plant Physiol 2012;160:1530–9. https://doi.org/10.1104/pp.112.204438.
[56] Tian H, Wang R, Li J, Zhao S, Teotia S, Gao B, et al. Regulation of rice grain weight by fatty acid composition: unveiling the mechanistic roles of *OsLIN6* by OsARF12. J Agric Food Chem 2024;72:24655–67. https://doi.org/10.1021/acs.jafc.4c06582.
[57] Fan J, Sah SK, Lemes Jorge G, Blanford J, Xie D, Yu L, et al. Arabidopsis trigalactosyldiacylglycerol1 mutants reveal a critical role for phosphtidylcholine remodeling in lipid homeostasis. Plant J 2024;120:788–98. https://doi.org/10.1111/tpj.17020.
[58] Focks N, Benning C. Wrinkled1: a novel, low-seed-oil mutant of Arabidopsis with a deficiency in the seed-specific regulation of carbohydrate metabolism. Plant Physiol 1998;118:91–101. https://doi.org/10.1104/pp.118.1.91.
[59] To A, Joubes J, Barthole G, Lecureuil A, Scagnelli A, Jasinski S, et al. WRINKLED transcription factors orchestrate tissue-specific regulation of fatty acid biosynthesis in Arabidopsis. Plant Cell 2012;24:5007–23. https://doi.org/10.1105/tpc.112.106120.
[60] Grimberg Å, Carlsson AS, Marttila S, Bhalerao R, Hofvander P. Transcriptional transitions in *Nicotiana benthamiana* leaves upon induction of oil synthesis by WRINKLED1 homologs from diverse species and tissues. BMC Plant Biol 2015;15:192. https://doi.org/10.1186/s12870-015-0579-1.
[61] Adhikari ND, Bates PD, Browse J. *WRINKLED1* rescues feedback inhibition of fatty acid synthesis in hydroxylase-expressing seeds. Plant Physiol 2016;171:179–91. https://doi.org/10.1104/pp.15.01906.
[62] Li D, Jin C, Duan S, Zhu Y, Qi S, Liu K, et al. MYB89 transcription factor represses seed oil accumulation. Plant Physiol 2017;173:1211–25. https://doi.org/10.1104/pp.16.01634.
[63] Kim I, Lee K-R, Park M-E, Kim HU. The seed-specific transcription factor DPBF2 modulates the fatty acid composition in seeds. Plant Direct 2022;6:e395. https://doi.org/10.1002/pld3.395.
[64] Wang J, Deng Y, Zhou Y, Liu D, Yu H, Zhou Y, et al. Full-length mRNA sequencing and gene expression profiling reveal broad involvement of natural antisense transcript gene pairs in pepper development and response to stresses. Plant J 2019;99:763–83. https://doi.org/10.1111/tpj.14351.
[65] Zhang Y, Li Y, Han B, Liu A, Xu W. Integrated lipidomic and transcriptomic analysis reveals triacylglycerol accumulation in castor bean seedlings under heat stress. Ind Crop Prod 2022;180:114702. https://doi.org/10.1016/j.indcrop.2022.114702.
[66] Zhao J, An J, Hwang D, Wu Q, Wang S, Gillespie RA, et al. The lipid A 1-phosphatase, LpxE, functionally connects multiple layers of bacterial envelope biogenesis. mBio 2019;10:e00886–19. https://doi.org/10.1128/mbio.00886-19.
[67] Regmi A, Shockey J, Kotapati HK, Bates PD. Oil-producing metabolons containing DGAT1 use separate substrate pools from those containing DGAT2 or PDAT1. Plant Physiol 2020;184:720–37. https://doi.org/10.1104/pp.20.00461.
[68] Xu Y, Caldo KMP, Jayawardhane K, Ozga JA, Weselake RJ, Chen G. A transferase interactome that may facilitate channeling of polyunsaturated fatty acid moieties from phosphatidylcholine to triacylglycerol. J Biol Chem 2019;294:14838–44. https://doi.org/10.1074/jbc.AC119.010601.
[69] Demski K, Jeppson S, Stymne S, Lager I. Phosphatidylcholine:diacylglycerol cholinephosphotransferase's unique regulation of castor bean oil quality. Plant Physiol 2022;189:2001–14. https://doi.org/10.1093/plphys/kiac209.
[70] Sandager L, Gustavsson MH, Stahl U, Dahlqvist A, Wiberg E, Banas A, et al. Storage lipid synthesis is non-essential in yeast. J Biol Chem 2002;277:6478–82. https://doi.org/10.1074/jbc.M109109200.
[71] Marmon SK, Sturtevant D, Herrfurth C, Chapman KD, Stymne S, Feussner I. Two acyltransferases contribute differently to linolenic acid levels in seed oil. Plant Physiol 2017;173:2081–95. https://doi.org/10.1104/pp.16.01865.
[72] Rauwerdink A, Kazlauskas RJ. How the same core catalytic machinery catalyzes 17 different reactions: the serine-histidine-aspartate catalytic triad of α/β-hydrolase fold enzymes. ACS Catal 2015;5:6153–76. https://doi.org/10.1021/acscatal.5b01539.
[73] Shrestha P, Kandel J, Tayara H, Chong KT. Post-translational modification prediction via prompt-based fine-tuning of a GPT-2 model. Nat Commun 2024;15:6699. https://doi.org/10.1038/s41467-024-51071-9.
[74] Helenius A, Aebi M. Roles of N-linked glycans in the endoplasmic reticulum. Annu Rev Biochem 2004;73:1019–49. https://doi.org/10.1146/annurev.biochem.73.011303.073752.
[75] Parchuri P, Bhandari S, Azeez A, Chen G, Johnson K, Shockey J, et al. Identification of triacylglycerol remodeling mechanism to synthesize unusual fatty acid containing oils. Nat Commun 2024;15:3547. https://doi.org/10.1038/s41467-024-47995-x.
[76] Bhandari S, Bates PD. Triacylglycerol remodeling in *Physaria fendleri* indicates oil accumulation is dynamic and not a metabolic endpoint. Plant Physiol 2021;187:799–815. https://doi.org/10.1093/plphys/kiab294.
[77] Bates PD, Shockey J. Towards rational control of seed oil composition: dissecting cellular organization and flux control of lipid metabolism. Plant Physiol 2025;197:kiae658. https://doi.org/10.1093/plphys/kiae658.
[78] Bates PD, Browse J. The pathway of triacylglycerol synthesis through phosphatidylcholine in Arabidopsis produces a bottleneck for the accumulation of unusual fatty acids in transgenic seeds. Plant J 2011;68:387–99. https://doi.org/10.1111/j.1365-313X.2011.04693.x.
[79] Park M-E, Lee K-R, Chen GQ, Kim HU. Enhanced production of hydroxy fatty acids in Arabidopsis seed through modification of multiple gene expression. Biotechnol Biofuels Bioprod 2022;15:66. https://doi.org/10.1186/s13068-022-02167-1.
[80] Sun Y, Liu B, Xue J, Wang X, Cui H, Li R, et al. Critical metabolic pathways and genes cooperate for epoxy fatty acid-enriched oil production in developing seeds of *Vernonia galamensis*, an industrial oleaginous plant. Biotechnol Biofuels 2022;15:21. https://doi.org/10.1186/s13068-022-02120-2.
[81] Wang J, Xu Y, Holic R, Yu X, Singer SD, Chen G. Improving the production of punicic acid in baker's yeast by engineering genes in acyl channeling processes and adjusting precursor supply. J Agric Food Chem 2021;69:9616–24. https://doi.org/10.1021/acs.jafc.1c03256.
[82] Wang J, Chen G. Engineering *Saccharomyces cerevisiae* for the production of punicic acid-rich yeast biomass. J Agric Food Chem 2024;72:23917–27. https://doi.org/10.1021/acs.jafc.4c08252.
[83] van Erp H, Bryant FM, Martin-Moreno J, Michaelson LV, Bhutada G, Eastmond PJ. Engineering the stereoisomeric structure of seed oil to mimic human milk fat. Proc Natl Acad Sci 2019;116:20947–52. https://doi.org/10.1073/pnas.1907915116.
[84] Bates PD, Johnson SR, Cao X, Li J, Nam J-W, Jaworski JG, et al. Fatty acid synthesis is inhibited by inefficient utilization of unusual fatty acids for glycerolipid assembly. Proc Natl Acad Sci USA 2014;111:1204–9. https://doi.org/10.1073/pnas.1318511111.
[85] Miquel M, James D, Dooner H, Browse J. Arabidopsis requires polyunsaturated lipids for low-temperature survival. Proc Natl Acad Sci USA 1993;90:6208–12. https://doi.org/10.1073/pnas.90.13.6208.
[86] Bai S, Engelen S, Denolf P, Wallis JG, Lynch K, Bengtsson JD, et al. Identification, characterization and field testing of *Brassica napus* mutants producing high-oleic oils. Plant J 2019;98:33–41. https://doi.org/10.1111/tpj.14195.
[87] Xu Y, Singer SD, Chen G. Protein interactomes for plant lipid biosynthesis and their biotechnological applications. Plant Biotechnol J 2023;21:1734–44. https://doi.org/10.1111/pbi.14027.
[88] Shockey J, Regmi A, Cotton K, Neil A, Browse J, Bates PD. Identification of Arabidopsis *GPAT9* (At5g60620) as an essential gene involved in triacyglycerol biosynthesis. Plant Physiol 2016;170:163–79. https://doi.org/10.1104/pp.15.00025.
[89] Bates P. The plant lipid metabolic network for assembly of diverse triacylglycerol molecular species. Advances in Botanical Research, vol. 101, Elsevier; 2022, p. 225–52. Doi: https://doi.org/10.1016/bs.abr.2021.07.003.